Metallic nanoparticles on waveguide structures: effects on waveguide mode properties and the promise of sensing applications

T. Cheng,[1] C. Rangan,[1,*] and J. E. Sipe[2]

[1]*Department of Physics, University of Windsor, Windsor, Ontario N9B 3P4, Canada*
[2]*Department of Physics and Institute of Optical Sciences, University of Toronto, Toronto, Ontario M5S 1A7, Canada*
**Corresponding author: rangan@uwindsor.ca*

Received August 15, 2012; accepted October 15, 2012;
posted January 10, 2013 (Doc. ID 174060); published February 28, 2013

We present a treatment of metallic nanoparticles on waveguide (WG) structures, treating the scenario where the spacing between the metallic nanoparticles is much less than the wavelength of light. We derive an effective medium treatment of the layer containing the nanoparticles, introducing transfer matrices for the layer. The coefficients of the transfer matrices take into account the interaction of the nanoparticles with each other, as well as local field corrections to the interaction of the nanoparticles with the material beneath them. Used with the WG mode pole expansions for the Fresnel coefficients of the WG structure, this allows for simple expressions for the shift and width of the WG mode resonance wave vector induced by the nanoparticles. As an example, we work out the simple case where the nanoparticles are treated as point dipoles, and use it to investigate the potential of this kind of structure for sensing applications.

OCIS codes: 240.3695, 230.7370, 250.5403, 230.4170.

1. INTRODUCTION

We present a theory for a novel (to our knowledge) type of sensor, employing noble-metal nanoparticles (NPs) on a waveguide (WG). NPs are immobilized on the surface of a planar WG, which is the interface between the guiding layer and the cladding layer, the latter typically being either air or a solvent. The presence of the NPs modifies the properties of the guided mode, and this modification itself is changed by the adsorption of a sensing target or the change in the bulk index of refraction of the cladding layer.

Since the seminal work of Lukosz and Tiefenthaler in 1983 [1], WG sensors have enjoyed a high degree of popularity (see the review by Mukundan *et al.* [2]). The fundamental principle of WG biosensing is the change in the incoupling angle (the angle at which light incident on the WG structure through a grating or prism couples into the WG mode) due to the surface modification of the interface. These sensors have been widely used for biosensing, because they naturally form components of integrated optics systems.

In a separate line of inquiry, gold nanoparticles (GNPs) have also been found to be amenable for biosensing [3], because they combine the advantage of the strong binding affinity of thiol groups to gold [4] with narrow and sensitive localized surface plasmon resonance (LSPR) spectra [5,6]. When GNPs are immobilized on a surface [7], they offer an increased sensitivity at smaller sample volumes and the potential of multiplexing and parallelization.

One of the earliest attempts at leveraging both the advantages of the WG and NP sensors (the optical integration as well as the narrow LSPR spectra) came from Busse *et al.* [8], who deposited functionalized GNPs on one of the arms of a Mach–Zender interferometer. The NPs are illuminated by the evanescent field of the WG, which excites the localized surface plasmons in the NPs. The evanescent field can have different polarizations, corresponding to the transverse electric (TE) and transverse magnetic (TM) WG modes. Since then, there have been several types of GNPs on planar WG sensors [9–14], each differing by the placement of the GNPs in relation to the WG surface, the arrangement of GNPs, and the detection signal. A comprehensive review of NP-on-WG sensors has recently been completed by Mittler [15].

The general theory behind our sensor model employs a dyadic Green function approach developed earlier to model optical multilayers [16,17]. On top of a multilayer structure we consider a region of height d much less than the wavelength λ of light, and with variations in the optical susceptibility that range over distances a in the plane also much less than λ. In practice this "selvedge" region will often be made of metal NPs, in an ordered array or a disordered structure; the length scales distinguish the structures we study from NP array sensors with interparticle spacing comparable to the wavelength of light [18–20], which use interferometric effects to produce narrow plasmon bands and significant field enhancements. Our general goal is to determine how the presence of this selvedge region modifies the dispersion relation of the WG modes, and how that modification is itself modified by the presence of analytes that such a structure could be used to detect.

The optical properties of arrays of NPs have been studied by many workers, often in the limit of treating each particle as a point dipole (see, e.g., [21,22]), and sometimes even in the presence of multilayer structures (see, e.g., [23,24]). Although in Section 3 on toy models below we also make the point dipole approximation for the NPs, the general formalism we

develop is not restricted to that approximation, and we feel it will have its most important applications in systems where the NPs are close enough to each other that such an approximation is not valid. Our strategy is to split the calculation of the optical response of the selvedge into two parts, one having to do with the near (electrostatic limit) fields, which must (in general) be done numerically, and one having to do with the radiative fields, which can be done analytically, given our assumption that d, $a \ll \lambda$. Since the near fields drop off with increasing distance from a source much faster than the radiative fields, this will simplify the numerical work considerably.

The assumption that d, $a \ll \lambda$ places our work in the general field of "homogenization," and a naïve approach would be to simply apply one of the current approaches (see, e.g., [25–28]) to homogenize a selvedge envisioned to be in free space, and with its effective optical properties thus characterized treat it simply as a new layer on top of the multilayer structure. But this is too simplistic. We find that the effective optical properties of the selvedge itself are affected by the presence of the multilayer structure on which it resides, through, for example, the image dipole moments in the layer below the selvedge. Thus the homogenization must be done explicitly in the presence of the underlying multilayer. In this work we take the selvedge to be on top of a layer of thickness comparable to the wavelength of light, to model devices created by electroless deposition or electron beam deposition on a WG structure; a generalization that we will turn to in a following communication will treat the selvedge positioned on top of a thinner first layer, to model devices created by organometallic chemical vapor deposition.

The outline of the rest of the paper is as follows. We develop the theory in Section 2, which culminates in identifying transfer matrices for the selvedge. These allow us to easily determine the optical properties of the selvedge on top of the multilayer structures. Since WG modes, or other such resonances, are characterized by poles in the Fresnel coefficients, including the selvedge through its transfer matrices allows us to identify expressions for the shift in the position and width of those resonances due to the selvedge. In Section 3 we illustrate our approach by working out the simple examples of a selvedge consisting of spheres modeled as point dipoles, in either a lattice or a disordered array. For completeness we also work out the limit of a selvedge consisting of a very thin layer itself; this last case can also be done exactly, of course, since it just adds another layer to the multilayer structure. We turn to sensing examples in Section 4. Here we look at how the presence of analytes further modifies the position and width of the WG mode. Even though we restrict ourselves to the point dipole approximation for the spheres in the selvedge, which we take to be metallic, we show that monitoring these changes could lead, in some instances, to a sensor with a much better sensitivity than the standard surface plasmon resonance (SPR) sensor and, despite the absorption of light in the metal NPs, to an enhancement in the sensitivity of the original WG sensor on which this new structure is based. We conclude in Section 5. Some of the mathematical details are relegated to appendices.

2. THEORY

The structure we consider is shown in Fig. 1. We suppose there is a medium with refractive index n_1 for the region

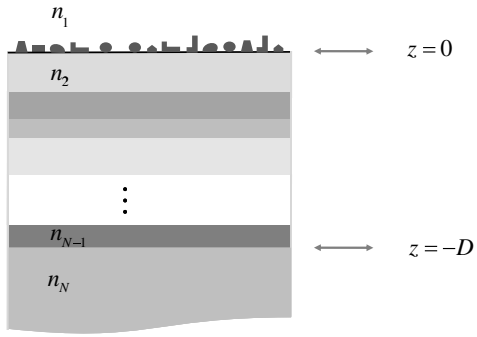

Fig. 1. Schematic of a multilayer structure with a medium (cladding) of refractive index n_1 above it. A selvedge layer of closely spaced GNPs lies along the interface between the multilayer and cladding.

$z > 0$ (the "cladding"), a multilayer in the region $-D < z < 0$ with $N - 1$ layers, and a medium with refractive index n_N in the region $z < -D$ (the "substrate"). We refer to this system alone, with complete translational invariance in the xy plane, as the "bare multilayer structure."

Added to this we suppose that nanostructures are added in the region $z > 0$, characterized by a susceptibility $\chi(\mathbf{r})$ that is only nonzero for $z > 0$, and describes the response *above and beyond* that associated with the uniform relative permittivity $\varepsilon_1 = n_1^2$. We take $\chi(\mathbf{r})$ to vanish for $z > d$ (see Fig. 2), and refer to the region $0 < z < d$ as the "selvedge." We put $\mathbf{r} = \mathbf{R} + z\hat{\mathbf{z}}$, where $\mathbf{R} = (x, y)$, write $\chi(\mathbf{r}) = \chi(\mathbf{R}; z)$, and generally use this notation for the position dependence of the fields.

A. Basic Equations

We take all the fields to be stationary at frequency ω:

$$f(\mathbf{R}; z; t) = f(\mathbf{R}; z)e^{-i\omega t} + \text{c.c.}$$

In particular, we take $\mathbf{E}(\mathbf{R}; z)$ to be the total electric field in the structure. The polarization $\mathbf{P}(\mathbf{R}; z)$ due to the additional susceptibility $\chi(\mathbf{R}; z)$ is given by

$$\mathbf{P}(\mathbf{R}; z) = \epsilon_0 \chi(\mathbf{R}; z)\mathbf{E}(\mathbf{R}; z). \tag{1}$$

This must be solved self-consistently, because $\mathbf{E}(\mathbf{R}; z)$ contains a contribution from the polarization $\mathbf{P}(\mathbf{R}; z)$ itself, which we write as $\mathbf{E}_p(\mathbf{R}; z)$; it can be expressed in terms of a Green function characterizing the solution of Maxwell's equations with a specified source $\mathbf{P}(\mathbf{R}; z)$ in the presence of the bare multilayer structure,

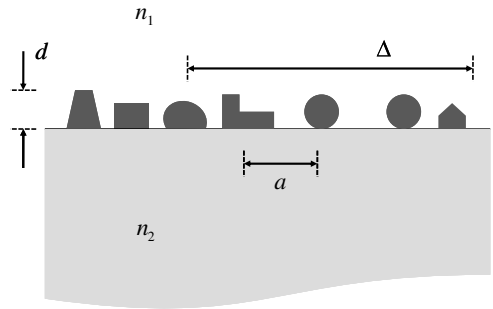

Fig. 2. Typical length scales in the problem. The thickness of the selvedge layer d and the interparticle spacing a are much smaller than the wavelength of light λ. Δ is a characteristic length scale such that $a \ll \Delta \ll \lambda$.

$$\mathbf{E}_p(\mathbf{R};z) = \int G(\mathbf{R}-\mathbf{R}';z,z')\cdot\mathbf{P}(\mathbf{R}';z')d\mathbf{R}'\mathrm{d}z', \tag{2}$$

and satisfying the usual outgoing radiation conditions at infinity. We can write the Green function $G(\mathbf{R}-\mathbf{R}';z,z')$ as the sum of two contributions,

$$G(\mathbf{R}-\mathbf{R}';z,z') = G^o(\mathbf{R}-\mathbf{R}';z,z') + G^R(\mathbf{R}-\mathbf{R}';z,z'), \tag{3}$$

where $G^o(\mathbf{R}-\mathbf{R}';z,z')$ (which in fact depends on only $\mathbf{R}-\mathbf{R}'$ and $z-z'$) is the Green function that would identify the electric field from a polarization placed in a uniform medium of relative permittivity $\epsilon_1 = n_1^2$, while $G^R(\mathbf{R}-\mathbf{R}';z,z')$ corrects for the presence of the multilayer structure. We give $G^o(\mathbf{R}-\mathbf{R}';z,z')$ in Appendix A and will present $G^R(\mathbf{R}-\mathbf{R}';z,z')$ later. The total electric field $\mathbf{E}(\mathbf{R};z)$ is then the sum of the particular solution $\mathbf{E}_p(\mathbf{R};z)$ and a homogeneous solution $\mathbf{E}_h(\mathbf{R};z)$ of the Maxwell equations for the bare multilayer structure:

$$\mathbf{E}(\mathbf{R};z) = \mathbf{E}_h(\mathbf{R};z) + \mathbf{E}_p(\mathbf{R};z). \tag{4}$$

In a simple example, $\mathbf{E}_h(\mathbf{R};z)$ might consist of a field incident on the bare multilayer structure from the cladding, as modified by all the reflected and transmitted fields that appear due to the interfaces. The polarization $\mathbf{P}(\mathbf{R};z)$ [Eq. (1)] then satisfies the integral equation:

$$\mathbf{P}(\mathbf{R};z) = \epsilon_0\chi(\mathbf{R};z)\Big(\mathbf{E}_h(\mathbf{R};z) + \int G(\mathbf{R}-\mathbf{R}';z,z')\cdot\mathbf{P}(\mathbf{R}';z')d\mathbf{R}'\mathrm{d}z'\Big). \tag{5}$$

In principle, once this is solved the full electric field [Eq. (4)] can be found everywhere using Eq. (2).

We take the homogeneous solution $\mathbf{E}_h(\mathbf{R};z)$ to be of the form

$$\mathbf{E}_h(\mathbf{R};z) = e^{i\kappa^i\cdot\mathbf{R}}\mathcal{F}_h(z), \tag{6}$$

where κ^i is a vector lying in the xy plane, $\kappa^i = (\kappa_x^i, \kappa_y^i)$. In the simple example of $\mathbf{E}_h(\mathbf{R};z)$ given above, Eq. (6) would correspond to an incident plane wave and κ^i would identify its components in the xy plane. Despite the complicated nature of the reflections and transmission at the interfaces, translational invariance of the bare multilayer structure guarantees that $\mathbf{E}_h(\mathbf{R};z)$ will be of the form Eq. (6). A more general $\mathbf{E}_h(\mathbf{R};z)$ can be described by taking $\mathbf{E}_h(\mathbf{R};z)$ to be a sum or integral of such terms, with different κ^i; the linearity of Eq. (5) would then allow us to find a complete solution by summing over those for different κ^i. For any κ^i of interest we take $\kappa^i = |\kappa^i|$ to be less than or on the order of $2\pi/\lambda$, where λ is the (vacuum) wavelength of light; in our simple example, assuming n_1 is real, $\kappa^i = 2\pi n_1 \sin\theta/\lambda$, where θ is the angle of incidence.

For an $\mathbf{E}_h(\mathbf{R};z)$ of the form in Eq. (6) we can without loss of generality write

$$\mathbf{P}(\mathbf{R};z) = e^{i\kappa^i\cdot\mathbf{R}}\mathbf{p}(\mathbf{R};z), \tag{7}$$

and we can solve Eq. (5) by solving

$$\mathbf{p}(\mathbf{R};z) = \epsilon_0\chi(\mathbf{R};z)\mathbf{F}(\mathbf{R};z), \tag{8}$$

where

$$\mathbf{F}(\mathbf{R};z) = \mathcal{F}_h(z) + \int e^{-i\kappa^i\cdot(\mathbf{R}-\mathbf{R}')}G(\mathbf{R}-\mathbf{R}';z,z')\cdot\mathbf{p}(\mathbf{R}';z')d\mathbf{R}'\mathrm{d}z', \tag{9}$$

and we leave the dependence of $\mathbf{F}(\mathbf{R};z)$ on κ^i implicit.

B. Assumptions

While we allow for some of the media in the multilayer structure to be absorbing, and therefore characterized by complex relative permittivities, for simplicity we consider the cladding to be transparent, with index n_1 real; without much practical restriction we take it to be of order unity. We will then construct an approximate solution of Eq. (8) under a number of assumptions that we will detail now (see Fig. 2). First, we assume the height of the selvedge region is much less than the wavelength λ of light in vacuum,

$$d \ll \lambda. \tag{10}$$

Next, we assume that inhomogeneities in $\chi(\mathbf{R};z)$ in the (xy) plane are characterized by a length scale a much less than λ, and further that we can identify a length scale Δ satisfying

$$a \ll \Delta \ll \lambda. \tag{11}$$

Finally, we assume that the κ^i of interest satisfy

$$\kappa^i\Delta \ll 1. \tag{12}$$

Note that for the simple example given above this is satisfied by virtue of Eq. (11), as it will be more generally for κ^i that will be of interest. We will make other assumptions that will restrict particular formulas that we will derive, but the general approach we adopt is restricted only by the assumptions characterized by Eqs. (10)–(12).

We now introduce a smooth nonnegative weighting function $W(\mathbf{R})$, peaking at $\mathbf{R}=0$, depending only on $R=|\mathbf{R}|$, nonzero over a range of R on the order of Δ, and normalized:

$$\int W(\mathbf{R})\mathrm{d}\mathbf{R} = 1.$$

Then consider the quantity

$$\int W(\mathbf{R}-\mathbf{R}')\mathbf{p}(\mathbf{R}';z)\mathrm{d}\mathbf{R}'. \tag{13}$$

Since by the assumptions in Eqs. (2) and (4) we expect inhomogeneities in $\mathbf{p}(\mathbf{R}';z)$ on the order of a in the (xy) plane, and since the range Δ of $W(\mathbf{R}-\mathbf{R}')$ is much greater than a, the dependence on $\mathbf{R}$ of the quantity from Eq. (13) will be much smoother than the dependence of $\mathbf{p}(\mathbf{R};z)$. If we have a periodic array of NPs, then $\chi(\mathbf{R};z)$ will be a periodic function of $\mathbf{R}$,

$$\chi(\mathbf{R};z) = \sum_{\mathbf{K}}\chi_{\mathbf{K}}(z)e^{i\mathbf{K}\cdot\mathbf{R}}, \tag{14}$$

where $\mathbf{K} = (K_x, K_y)$ are reciprocal lattice vectors, and so will be $\mathbf{p}(\mathbf{R};z)$:

$$\mathbf{p}(\mathbf{R};z)=\sum_{\mathbf{K}}\mathbf{p}_{\mathbf{K}}(z)e^{i\mathbf{K}\cdot\mathbf{R}}. \tag{15}$$

Since other than $\mathbf{K}=0$ the smallest $K=|\mathbf{K}|$ is of order $1/a$, to good approximation only the $\mathbf{K}=0$ term will survive in Eq. (15), and to this approximation that quantity will be independent of $\mathbf{R}$. Even if we have a disordered array of NPs, we assume that disorder is such than when averaged over Δ as in Eq. (13), we have a uniform result, to good approximation. So we take

$$\mathcal{P}(z)\equiv\int W(\mathbf{R}-\mathbf{R}')\mathbf{p}(\mathbf{R}';z)\mathrm{d}\mathbf{R}' \tag{16}$$

to be independent of $\mathbf{R}$. We put

$$\tilde{\mathbf{p}}(\mathbf{R};z)\equiv\mathbf{p}(\mathbf{R};z)-\mathcal{P}(z), \tag{17}$$

and we also define

$$\mathbf{Q}\equiv\int\mathcal{P}(z)\mathrm{d}z. \tag{18}$$

C. Coarse-Grained Fields

In a similar way it will be useful to use the function $W(\mathbf{R}-\mathbf{R}')$ to introduce coarse-grained fields more generally. For example, for the full electric field [Eqs. (2), (4)] we can introduce an electric field coarse-grained in the plane,

$$\bar{\mathbf{E}}(\mathbf{R};z)\equiv\int W(\mathbf{R}-\mathbf{R}')\mathbf{E}(\mathbf{R}';z)\mathrm{d}\mathbf{R}'. \tag{19}$$

Of course, the coarse-grained field $\bar{\mathbf{E}}(\mathbf{R};z)$ cannot be used in place of $\mathbf{E}(\mathbf{R};z)$ to determine the polarization [Eq. (5)]; variations on the order of $a\ll\Delta$ are important. However, it suffices to know $\bar{\mathbf{E}}(\mathbf{R};z)$ over planes at $z>d$ and $z<0$ if we want to determine even the full electric field as $z\to\pm\infty$. Here is why: in a Fourier decomposition of $\mathbf{E}(\mathbf{R};z)$ in the xy plane,

$$\mathbf{E}(\mathbf{R};z)=\int\frac{\mathrm{d}\kappa}{(2\pi)^2}\mathbf{E}(\kappa;z)e^{i\kappa\cdot\mathbf{R}}, \tag{20}$$

where $\kappa=(\kappa_x,\kappa_y)$, only the components with $\kappa\equiv|\kappa|<2\pi n_1/\lambda$ (for $z\to\infty$) and $\kappa<2\pi n_N/\lambda$ (for $z\to-\infty$) will be important for those far fields. They are not affected by the coarse-graining, since $\Delta\ll\lambda$, so specifying $\bar{\mathbf{E}}(\mathbf{R};z)$ identifies them completely. Because of this, $\bar{\mathbf{E}}(\mathbf{R};z)$ will be a useful field, as we will see in detail below.

Defining other averages in the same way, from Eqs. (4) and (19) we have

$$\bar{\mathbf{E}}(\mathbf{R};z)=\bar{\mathbf{E}}_h(\mathbf{R};z)+\bar{\mathbf{E}}_p(\mathbf{R};z).$$

From Eq. (6) and the fact that κ^i satisfies Eq. (12), the spatial average of the field $\mathbf{E}_h(\mathbf{R};z)$ is essentially equal to the field itself, and we can take

$$\bar{\mathbf{E}}_h(\mathbf{R};z)\simeq\mathbf{E}_h(\mathbf{R};z)=e^{i\kappa^i\cdot\mathbf{R}}\mathcal{F}_h(z). \tag{21}$$

From Eq. (2) we have

$$\begin{aligned}\bar{\mathbf{E}}_p(\mathbf{R};z)&=\int W(\mathbf{R}-\mathbf{R}')G(\mathbf{R}'-\mathbf{R}'';z,z')\cdot\mathbf{P}(\mathbf{R}'';z')d\mathbf{R}'d\mathbf{R}''\mathrm{d}z'\\&=\int G(\mathbf{R}-\mathbf{R}''';z,z')\cdot\bar{\mathbf{P}}(\mathbf{R}''';z')d\mathbf{R}'''\mathrm{d}z',\end{aligned} \tag{22}$$

where in the second line we have eliminated the variable $\mathbf{R}'$ in favor of a new variable $\mathbf{R}'''=\mathbf{R}-\mathbf{R}'+\mathbf{R}''$ and defined $\bar{\mathbf{P}}(\mathbf{R};z)$ in terms of $\mathbf{P}(\mathbf{R};z)$ according to the pattern of Eq. (19). From Eqs. (7) and (16) we see that

$$\bar{\mathbf{P}}(\mathbf{R}''';z')\approx e^{i\kappa^i\cdot\mathbf{R}'''}\mathcal{P}(z'),$$

and so

$$\begin{aligned}\bar{\mathbf{E}}_p(\mathbf{R};z)&=\int G(\mathbf{R}-\mathbf{R}''';z,z')\cdot e^{i\kappa^i\cdot\mathbf{R}'''}\mathcal{P}(z')d\mathbf{R}'''\mathrm{d}z'\\&=e^{i\kappa^i\cdot\mathbf{R}}\int G(\kappa^i;z,z')\cdot\mathcal{P}(z')\mathrm{d}z',\end{aligned}$$

where we introduce a Fourier decomposition in the xy plane of all our Green functions,

$$\begin{aligned}G(\mathbf{R};z,z')&=\int\frac{\mathrm{d}\kappa}{(2\pi)^2}G(\kappa;z,z')e^{i\kappa\cdot\mathbf{R}},\\G^{o,R}(\mathbf{R};z,z')&=\int\frac{\mathrm{d}\kappa}{(2\pi)^2}G^{o,R}(\kappa;z,z')e^{i\kappa\cdot\mathbf{R}},\end{aligned} \tag{23}$$

[recall Eq. (3)]. Combining Eqs. (21) and (22), we find

$$\bar{\mathbf{E}}(\mathbf{R};z)=e^{i\kappa^i\cdot\mathbf{R}}\Big(\mathcal{F}_h(z)+\int G(\kappa^i;z,z')\cdot\mathcal{P}(z')\mathrm{d}z'\Big). \tag{24}$$

So within our assumptions the dependence of $\bar{\mathbf{E}}(\mathbf{R};z)$ on $\mathbf{R}$ is completely captured by the phase factor $e^{i\kappa^i\cdot\mathbf{R}}$.

D. Terms in the Integral Equation

After these preliminaries we are ready to use our assumptions to simplify the terms appearing in Eqs. (8) and (9). Using Eq. (3) we write Eq. (9) as

$$\mathbf{F}(\mathbf{R};z)=\mathcal{F}_h(z)+\mathbf{F}^o(\mathbf{R},z)+\mathbf{F}^R(\mathbf{R},z), \tag{25}$$

where

$$\mathbf{F}^{o,R}(\mathbf{R},z)\equiv\int e^{-i\kappa^i\cdot(\mathbf{R}-\mathbf{R}')}G^{o,R}(\mathbf{R}-\mathbf{R}';z,z')\cdot\mathbf{p}(\mathbf{R}';z')d\mathbf{R}'\mathrm{d}z'. \tag{26}$$

We look at these individual terms. The first step will be to move toward expressing these individual terms in terms of spatially averaged fields as far as possible; this will help us construct an equation for $\mathbf{p}(\mathbf{R};z)$ in terms of $\mathcal{F}_h(z)$ and $\mathcal{P}(z)$. The second step will then be to use this to derive a self-consistent equation for $\mathbf{Q}$, which we will see will be instrumental in determining the fields everywhere in the structure.

In implementing the first step, we very broadly follow the original approach of Lorentz to describe the constitutive relations of macroscopic media [29]. For example, we divide the integral [Eq. (26)] involving G^o into two integrals, one over $\mathbf{R}'$ satisfying $|\mathbf{R}'-\mathbf{R}|>\Delta$ and one over $\mathbf{R}'$ satisfying $|\mathbf{R}'-\mathbf{R}|<\Delta$. In the first of these we relate the contribution of $\mathbf{p}(\mathbf{R}';z')$ to $\bar{\mathbf{E}}(\mathbf{R};z)$. In the second we can use expressions for the longitudinal component of the electric field, and for the transverse component in the range $|\mathbf{R}'-\mathbf{R}|<\lambda$, to simplify the analysis.

Indeed, the problem here is in a sense simpler than Lorentz' original problem because the longitudinal dipole field, dropping off as $|\mathbf{R}' - \mathbf{r}|^{-3}$, is more benign in our quasi-two-dimensional geometry (volume element $RdRd\phi dz$, with $0 < R < \infty$ but $0 < z < d$) than in the full three-dimensional geometry (volume element $r^2 dr d\Omega$, with $0 < r < \infty$). No correction to the local field of the form $\mathbf{P}/3\epsilon_0$ that arises in the three-dimensional problem (see Eq. (4.20) of [30]) appears here. But the lattice sum correction that vanishes in a three-dimensional cubic lattice, and thus is usually neglected in three-dimensional problems, generally does not vanish in a two-dimensional lattice, even if it is cubic, and so it appears here. And in another sense our problem is more complicated than the usual analysis for a macroscopic three-dimensional medium: we have an additional contribution, the integral [Eq. (26)] involving G^R that describes reflection from the underlying multilayer. Besides providing a correction to the transverse field in the selvedge, this also provides a longitudinal component that can be associated with image dipoles in the layer beneath the selvedge, as we see below.

We begin this analysis with $\mathbf{F}^o(\mathbf{R}, z)$, writing it as the sum of the two terms indicated above,

$$\mathbf{F}^o(\mathbf{R}, z) = \mathbf{F}^>(\mathbf{R}, z) + \mathbf{F}^<(\mathbf{R}, z), \tag{27}$$

where

$$\mathbf{F}^{\gtrless}(\mathbf{R}, z) \equiv \int_{|\mathbf{R}'-\mathbf{R}|\gtrless\Delta} e^{-i\kappa^i\cdot(\mathbf{R}-\mathbf{R}')} G^o(\mathbf{R}-\mathbf{R}'; z, z') \cdot \mathbf{p}(\mathbf{R}'; z') d\mathbf{R}' dz'. \tag{28}$$

In the first of these, the inhomogeneities of $\mathbf{p}(\mathbf{R}'; z')$ are on the order of $a \ll \Delta$, and their effect on the value of the integral at $\mathbf{R}$ such that $|\mathbf{R} - \mathbf{R}'| > \Delta$ will be negligible, since for such $\mathbf{R}$ the integrand $e^{-i\kappa^i\cdot(\mathbf{R}-\mathbf{R}')} G^o(\mathbf{R}-\mathbf{R}'; z, z')$ will vary little as $\mathbf{R}'$ ranges over distances of order a [see Eqs. (11) and (12) and Eq. (A1) of Appendix A]. So we can replace $\mathbf{p}(\mathbf{R}'; z')$ simply by $\mathcal{P}(z')$. We then can write

$$\begin{aligned}\mathbf{F}^>(\mathbf{R}, z) = &\int_{|\mathbf{R}'-\mathbf{R}|>\Delta} (e^{-i\kappa^i\cdot(\mathbf{R}-\mathbf{R}')} - 1) G^o(\mathbf{R}-\mathbf{R}'; z, z') \\ &\cdot \mathcal{P}(z') d\mathbf{R}' dz' + \int_{|\mathbf{R}'-\mathbf{R}|>\Delta} G^o(\mathbf{R}-\mathbf{R}'; z, z') \\ &\cdot \mathcal{P}(z') d\mathbf{R}' dz'.\end{aligned}$$

In the first of the terms we can extend the integral over all $\mathbf{R}'$, since for $|\mathbf{R}' - \mathbf{R}| < \Delta$ we have $(e^{-i\kappa^i\cdot(\mathbf{R}-\mathbf{R}')} - 1) \approx 0$. So

$$\begin{aligned}\mathbf{F}^>(\mathbf{R}, z) = &\int (G^o(\kappa^i; z, z') - G^o(0; z, z')) \cdot \mathcal{P}(z') dz' \\ &+ \int_{|\mathbf{R}'-\mathbf{R}|>\Delta} G^o(\mathbf{R}-\mathbf{R}'; z, z') \cdot \mathcal{P}(z') d\mathbf{R}' dz',\end{aligned}$$

where $G^o(0; z, z')$ denotes $G^o(\kappa; z, z')$ [Eq. (23)] at $\kappa = 0$. Again using $e^{-i\kappa^i\cdot(\mathbf{R}-\mathbf{R}')} \approx 1$ for $|\mathbf{R}' - \mathbf{R}| < \Delta$ in the second term of of Eq. (28), from Eq. (27) we have

$$\begin{aligned}\mathbf{F}^o(\mathbf{R}, z) = &\int_{|\mathbf{R}'-\mathbf{R}|<\Delta} G^o(\mathbf{R}-\mathbf{R}'; z, z') \cdot \mathbf{p}(\mathbf{R}'; z') d\mathbf{R}' dz' \\ &+ \int_{|\mathbf{R}'-\mathbf{R}|>\Delta} G^o(\mathbf{R}-\mathbf{R}'; z, z') \cdot \mathcal{P}(z') d\mathbf{R}' dz' \\ &+ \int (G^o(\kappa^i; z, z') - G^o(0; z, z')) \cdot \mathcal{P}(z') dz'. \end{aligned} \tag{29}$$

For use in the first two terms on the right-hand side of this equation, we now decompose $G^o(\mathbf{R} - \mathbf{R}'; z, z')$ into the part that identifies the longitudinal component of the generated electric field, $G^o_L(\mathbf{R} - \mathbf{R}'; z, z')$, and the part that identifies the transverse component of the generated electric field, $G^o_T(\mathbf{R} - \mathbf{R}'; z, z')$:

$$G^o(\mathbf{R} - \mathbf{R}'; z, z') = G^o_L(\mathbf{R} - \mathbf{R}'; z, z') + G^o_T(\mathbf{R} - \mathbf{R}'; z, z') \tag{30}$$

(see Appendix A); we can construct Fourier components of these new quantities, $G^o_L(\kappa; z, z')$ and $G^o_T(\kappa; z, z')$, just as we did for the full $G^o(\mathbf{R}; z, z')$ [Eq. (23)], with of course

$$G^o(\kappa^i; z, z') = G^o_T(\kappa^i; z, z') + G^o_L(\kappa^i; z, z'). \tag{31}$$

For $|\mathbf{R}' - \mathbf{R}| < \Delta$ we have

$$4\pi\epsilon_0 G^o_T(\mathbf{R} - \mathbf{R}'; z, z') = \frac{\tilde{\omega}^2}{2r}(U + \hat{\mathbf{r}}\,\hat{\mathbf{r}}) + \frac{2}{3} i\tilde{\omega}^3 n_1 U + \cdots, \tag{32}$$

(see Appendix A), where $\mathbf{r} = (\mathbf{R} - \mathbf{R}') + \hat{\mathbf{z}}(z - z')$. For our ranges [Eq. (11)], the first (real) term in Eq. (32), when used in the first term of Eq. (29), will typically lead to a much smaller contribution than that arising from the first (and also real) term in $G^o_L(\mathbf{R} - \mathbf{R}'; z, z')$ [see Eq. (A2) of Appendix A], to which it must ultimately be added. And so we drop it. The second term in Eq. (32) is imaginary, and it imposes energy conservation by radiation reaction (see Ch. 16 of [30]) on the oscillating polarization; so we keep it. But it is uniform, and so when it is inserted in the first term of Eq. (29) we can replace $\mathbf{p}(\mathbf{R}'; z')$ by $\mathcal{P}(z')$. Then, adding the contribution to the first two terms in Eq. (29) from $G^o_T(\mathbf{R} - \mathbf{R}'; z, z')$, we can do the integrals over $\mathbf{R}'$ to find a term that cancels out the transverse contribution to $G^o(0; z, z')$ in the last term of Eq. (29). Finally, in evaluating the longitudinal contribution to the first two lines [Eq. (29)], we note that $G^o_L(\mathbf{R} - \mathbf{R}'; z, z')$ drops off as $(|\mathbf{R} - \mathbf{R}'|^2 + (z - z')^2)^{-3/2}$ [see Eq. (A2) of Appendix A]; Δ is much larger than typical inter-unit spacing a according to our second assumption [Eq. (11)], and so in these longitudinal contributions in which lambda does not appear, we can let Δ go to infinity to find

$$\begin{aligned}\mathbf{F}^o(\mathbf{R}, z) = &\int G^o_L(\mathbf{R} - \mathbf{R}'; z, z') \cdot \mathbf{p}(\mathbf{R}'; z') d\mathbf{R}' dz' \\ &+ \int (G^o(\kappa^i; z, z') - G^o_L(0; z, z')) \cdot \mathcal{P}(z') dz', \end{aligned} \tag{33}$$

where we have used Eq. (31).

We next turn to Eq. (26) for $\mathbf{F}^R(\mathbf{R}; z)$. We separate the contributions to $\mathbf{F}^R(\mathbf{R}; z)$ from the terms $\mathcal{P}(z)$ and $\tilde{\mathbf{p}}(\mathbf{R}; z)$ that constitute $\mathbf{p}(\mathbf{R}; z)$ [recall Eq. (17)] by writing

$$\mathbf{F}^R(\mathbf{R}, z) = \bar{\mathbf{F}}^R(\mathbf{R}, z) + \tilde{\mathbf{F}}^R(\mathbf{R}, z), \tag{34}$$

where

$$\begin{aligned}\bar{\mathbf{F}}^R(\mathbf{R}, z) &= \int e^{-i\kappa^i\cdot(\mathbf{R}-\mathbf{R}')} G^R(\mathbf{R} - \mathbf{R}'; z, z') \cdot \mathcal{P}(z') d\mathbf{R}' dz' \\ &= \int G^R(\kappa^i; z, z') \cdot \mathcal{P}(z') dz', \end{aligned} \tag{35}$$

$$\tilde{\mathbf{F}}^R(\mathbf{R},z)=\int e^{-i\kappa^i\cdot(\mathbf{R}-\mathbf{R}')}G^R(\mathbf{R}-\mathbf{R}';z,z')\cdot\tilde{\mathbf{p}}(\mathbf{R}';z')d\mathbf{R}'dz'.$$

For the first of these we have

$$\tilde{\mathbf{F}}^R(\mathbf{R},z)=\frac{i\tilde{\omega}^2}{2\varepsilon_0 w_1^i}e^{iw_1^i z}(\hat{\mathbf{s}}^i R^s_{1N}(\kappa^i)\hat{\mathbf{s}}^i+\hat{\mathbf{p}}^i_{1+}R^p_{1N}(\kappa^i)\hat{\mathbf{p}}^i_{1-})\cdot\int e^{iw_1^i z'}\mathcal{P}(z')dz', \tag{36}$$

where we have introduced a number of new terms, and we begin by defining them. In general we use w_l to characterize the z dependence of plane waves in medium l with wave vector component κ in the (xy) plane; so $w_l=w_l(\kappa)$ with

$$w_l=\sqrt{\tilde{\omega}^2\varepsilon_l-\kappa^2}, \tag{37}$$

with $\tilde{\omega}\equiv\omega/c$, and defined so $\mathrm{Im}\,w_l\geq 0$, and if $\mathrm{Im}\,w_l=0$ then $\mathrm{Re}\,w_l\geq 0$; in Eq. (36) and elsewhere w_1^i indicates $w_1(\kappa^i)$. There are upward-propagating (or evanescent, if w_l has an imaginary component) waves (z dependence $e^{iw_l z}$) and downward-propagating (or evanescent) waves (z dependence $e^{-iw_l z}$) that are components of the homogeneous solution of Maxwell's equations in medium l for a given κ. We use $\hat{\mathbf{s}}$ to indicate the polarization vector for s-polarized light,

$$\hat{\mathbf{s}}\equiv\hat{\kappa}\times\hat{\mathbf{z}}, \tag{38}$$

characterized by κ, while $\hat{\mathbf{p}}_{l+}$ and $\hat{\mathbf{p}}_{l-}$ are the unit vectors for, respectively, upward and downward p-polarized light in medium l characterized by κ,

$$\hat{\mathbf{p}}_{l\pm}\equiv\frac{\kappa\hat{\mathbf{z}}\mp w_l\hat{\kappa}}{\tilde{\omega}n_l} \tag{39}$$

with $n_l=\sqrt{\varepsilon_l}$. The superscripts i appearing in Eq. (36) indicate that the vectors are to be evaluated at κ^i; $R^s_{1N}(\kappa^i)$ and $R^p_{1N}(\kappa^i)$ are, respectively, the reflection coefficients from the bare multilayer structure for a beam incident from medium 1 at κ^i (See Appendix B). The result [Eq. (36)] follows from the identification of $G^R(\kappa;z,z')$ that is given in Appendix B, and the physics behind the terms can be simply understood as described there. To determine $\tilde{\mathbf{F}}^R(\mathbf{R},z)$, it is convenient to write

$$\tilde{\mathbf{F}}^R(\mathbf{R},z)=\tilde{\mathbf{F}}^R_I(\mathbf{R},z)+\tilde{\mathbf{F}}^R_C(\mathbf{R},z), \tag{40}$$

where

$$\tilde{\mathbf{F}}^R_{I,C}(\mathbf{R},z)\equiv\int e^{-i\kappa^i\cdot(\mathbf{R}-\mathbf{R}')}G^R_{I,C}(\mathbf{R}-\mathbf{R}';z,z')\cdot\tilde{\mathbf{p}}(\mathbf{R}';z')d\mathbf{R}'dz', \tag{41}$$

where in Fourier space

$$G^R(\kappa;z,z')=G^R_I(\kappa;z,z')+G^R_C(\kappa;z,z'). \tag{42}$$

$G^R_I(\kappa;z,z')$ is defined as the double limit of $G^R(\kappa;z,z')$ as $\kappa c/\omega\to\infty$ *and* $\kappa D_2\to\infty$, where D_2 is the thickness of the layer (relative permittivity ε_2) directly below the cladding (relative permittivity ε_1). This limit of the Green function corresponds to electrostatics, with the selvedge above an infinitely thick medium of relative permittivity ε_2; so it is not surprising that $\tilde{\mathbf{F}}^R_I(\mathbf{R},z)$ is associated with the image polarization of $\tilde{\mathbf{p}}(\mathbf{R};z)$ in the layer below the selvedge,

$$\tilde{\mathbf{p}}^I(\mathbf{R};z)\equiv\frac{\varepsilon_2-\varepsilon_1}{\varepsilon_2+\varepsilon_1}(\hat{\mathbf{z}}\,\hat{\mathbf{z}}-\hat{\mathbf{x}}\,\hat{\mathbf{x}}-\hat{\mathbf{y}}\,\hat{\mathbf{y}})\cdot\tilde{\mathbf{p}}(\mathbf{R};-z) \tag{43}$$

for $z<0$; we have

$$\tilde{\mathbf{F}}^R_I(\mathbf{R},z)=\int e^{-i\kappa^i\cdot(\mathbf{R}-\mathbf{R}')}G^o_L(\mathbf{R}-\mathbf{R}';z,z')\cdot\tilde{\mathbf{p}}^I(\mathbf{R}',z')dz'd\mathbf{R}'$$

as we show in Appendix C. Using the same strategy we used above for reducing $\mathbf{F}_<(\mathbf{R},z)$, in place of Eq. (29) we find

$$\begin{aligned}\tilde{\mathbf{F}}^R_I(\mathbf{R},z)&=\int_{|\mathbf{R}'-\mathbf{R}|<\Delta}G^o_L(\mathbf{R}-\mathbf{R}';z,z')\cdot\tilde{\mathbf{p}}^I(\mathbf{R}';z')d\mathbf{R}'dz'\\&\to\int G^o_L(\mathbf{R}-\mathbf{R}';z,z')\cdot\tilde{\mathbf{p}}^I(\mathbf{R}';z')d\mathbf{R}'dz'\\&\to\int G^o_L(\mathbf{R}-\mathbf{R}';z,z')\cdot\mathbf{p}^I(\mathbf{R}';z')d\mathbf{R}'dz',\end{aligned} \tag{44}$$

where the first term on the right-hand side is simpler than that on the right-hand side of Eq. (29), since the spatial average over Δ of $\tilde{\mathbf{p}}(\mathbf{R};z)$ vanishes [recall Eq. (17)], and thus so does that of $\tilde{\mathbf{p}}^I(\mathbf{R};z)$. The first reduction on the right-hand side of Eq. (44) results because of the rapid drop off of $G^o_L(\mathbf{R}-\mathbf{R}';z,z')$ with $|\mathbf{R}-\mathbf{R}'|$ [already used in the corresponding simplification of Eq. (29), as discussed just before Eq. (33)], and the second reduction on the right-hand side of Eq. (44), where

$$\mathbf{p}^I(\mathbf{R};z)\equiv\frac{\varepsilon_2-\varepsilon_1}{\varepsilon_2+\varepsilon_1}(\hat{\mathbf{z}}\,\hat{\mathbf{z}}-\hat{\mathbf{x}}\,\hat{\mathbf{x}}-\hat{\mathbf{y}}\,\hat{\mathbf{y}})\cdot\mathbf{p}(\mathbf{R};-z) \tag{45}$$

arises because for $z>0$ and $z<0$ the $\kappa=0$ component of $G^o_L(\kappa;z,z')$ vanishes [see Eq. (C3) of Appendix C]. Combining Eqs. (34), (36), (40), (41), and (44), we then have

$$\begin{aligned}\mathbf{F}^R(\mathbf{R},z)=&\int G^o_L(\mathbf{R}-\mathbf{R}';z,z')\cdot\mathbf{p}^I(\mathbf{R}';z')d\mathbf{R}'dz'\\&+\frac{i\tilde{\omega}^2}{2\varepsilon_0 w_1^i}e^{iw_1^i z}(\hat{\mathbf{s}}^i R^s_{1N}(\kappa^i)\hat{\mathbf{s}}^i\\&+\hat{\mathbf{p}}^i_{1+}R^p_{1N}(\kappa^i)\hat{\mathbf{p}}^i_{1-})\cdot\int e^{iw_1^i z'}\mathcal{P}(z')dz'\\&+\int e^{-i\kappa^i\cdot(\mathbf{R}-\mathbf{R}')}G^R_C(\mathbf{R}-\mathbf{R}';z,z')\\&\cdot\tilde{\mathbf{p}}(\mathbf{R}';z')d\mathbf{R}'dz'.\end{aligned} \tag{46}$$

Now we turn to the last term in Eq. (46). Consider first the case of a lattice of NPs, where the function $\mathbf{p}(\mathbf{R};z)$ is periodic in z [Eq. (15)]:

$$\tilde{\mathbf{p}}(\mathbf{R};z)=\sum_{\mathbf{K}\neq 0}\mathbf{p}_{\mathbf{K}}(z)e^{i\mathbf{K}\cdot\mathbf{R}},$$

since in forming $\tilde{\mathbf{p}}(\mathbf{R};z)$ we essentially remove the uniform component of $\mathbf{p}(\mathbf{R};z)$ [see Eqs. (16) and (17) and the preceding discussion]. Then

$$\int e^{-i\kappa^i\cdot(\mathbf{R}-\mathbf{R}')}G_C^R(\mathbf{R}-\mathbf{R}';z,z')\cdot\tilde{\mathbf{p}}(\mathbf{R}';z')d\mathbf{R}'dz'$$
$$=\sum_{\mathbf{K}\neq 0}e^{i\mathbf{K}\cdot\mathbf{R}}\int e^{-i(\kappa^i+\mathbf{K})\cdot(\mathbf{R}-\mathbf{R}')}G_C^R(\mathbf{R}-\mathbf{R}';z,z')\cdot\mathbf{p}_{\mathbf{K}}(z')d\mathbf{R}'dz'$$
$$=\sum_{\mathbf{K}\neq 0}e^{i\mathbf{K}\cdot\mathbf{R}}\int G_C^R(\kappa^i+\mathbf{K};z,z')\cdot\mathbf{p}_{\mathbf{K}}(z')dz'. \quad (47)$$

Recalling that for nonzero $\mathbf{K}$ we have K on the order of $1/a$, we certainly have $|\kappa^i+\mathbf{K}|c/\omega \gtrsim c/(\omega a)\gg 1$ by Eq. (11); if as well we have $D_2/a\gg 1$, then $|\kappa^i+\mathbf{K}|D_2\gg 1$, and by definition $G_C^R(\kappa^i+\mathbf{K};z,z')$ will be negligible and the integral [Eq. (47)] will essentially vanish. Recalling Eq. (11), this latter inequality will be satisfied for D_2 on the order of a wavelength of light. This is the usual size of layers in typical thin-film multilayer structures, and so we assume that the latter inequality is indeed satisfied. However, if it were not satisfied, the extra contributions due to Eq. (47) could be easily worked out; they correspond to further image terms in lower layers of the structure. For $D_2/a\gg 1$ the field from these secondary image dipoles in layers below the first beneath the cladding will be so far away from the selvedge that their contribution will be negligible.

For a disordered medium, but where the disorder is not too great, for $D_2/a\gg 1$ we may take Eq. (47) to vanish to good approximation as well; alternately, we may make a mean field approximation and replace $\mathbf{p}(\mathbf{R};z)$ by its average value $\mathcal{P}(z)$; then $\tilde{\mathbf{p}}(\mathbf{R}';z')$ itself vanishes, and so does the term [Eq. (47)].

Finally returning to Eq. (25), we can combine the results [Eqs. (33), (46)], and the assumption that Eq. (47) vanishes, to write

$$\mathbf{F}(\mathbf{R};z)=\mathcal{F}_{h+}e^{iw_1^iz}+\mathcal{F}_{h-}e^{-iw_1^iz}$$
$$+\int G_L^o(\mathbf{R}-\mathbf{R}';z,z')\cdot(\mathbf{p}(\mathbf{R}';z')+\mathbf{p}^I(\mathbf{R}';z'))d\mathbf{R}'dz'$$
$$+\int(G^o(\kappa^i;z,z')-G_L^o(0;z,z'))\cdot\mathcal{P}(z')dz'$$
$$+\frac{i\tilde{\omega}^2}{2\varepsilon_0 w_1^i}e^{iw_1^iz}(\hat{\mathbf{s}}^iR_{1N}^s(\kappa^i)\hat{\mathbf{s}}^i$$
$$+\hat{\mathbf{p}}_{1+}^iR_{1N}^p(\kappa^i)\hat{\mathbf{p}}_{1-}^i)\cdot\int e^{iw_1^iz'}\mathcal{P}(z')dz', \quad (48)$$

where recalling the form of the homogeneous solution [Eq. (6)], we have used the fact that $\mathcal{F}_h(z)$ must consist of an upward component varying with z as $e^{iw_1^iz}$ (amplitude $\mathcal{F}_{h+}$) and a downward component varying with z as $e^{-iw_1^iz}$ (amplitude $\mathcal{F}_{h-}$); see the discussion around Eq. (37).

The physics of the different terms in Eq. (48) can now be identified. The last term describes the coarse-grained field in the selvedge that is due to the field from the selvedge itself reflected from the bare multilayer. The correction to this coarse-grained field is the integral involving $\mathbf{p}^I(\mathbf{R}';z')$ in Eq. (48), which describes the longitudinal field from the image polarization in medium 2. The integral involving $\mathbf{p}(\mathbf{R}';z')$ in Eq. (48) describes the longitudinal field in the selvedge from the selvedge itself. Both the integrals involving $\mathbf{p}(\mathbf{R}';z')$ and $\mathbf{p}^I(\mathbf{R}';z')$ give the longitudinal field in the approximation that $\kappa^i=0$; corrections to the integral involving $\mathbf{p}^I(\mathbf{R}';z')$ are included in the last term of Eq. (48), while corrections to the integral involving $\mathbf{p}(\mathbf{R}';z')$, along with the effects of the transverse field of the selvedge itself in the selvedge, are included in the third line of Eq. (48).

Based on the inequalities $w_1^iz, w_1^iz', \kappa^iz, \kappa^iz'\ll 1$ that follow from Eqs. (10) and (12), we can perform one further set of reductions of Eq. (48). From the last paragraph of Appendix C, using Eq. (31) and the expression [Eq. (C7)] for $G_T^o(\kappa^i;z,z')$ that holds in this limit, we find

$$\mathbf{F}(\mathbf{R};z)=\mathcal{F}'_{h+}(\kappa^i)+\mathcal{F}'_{h-}(\kappa^i)+G_S(\kappa^i)\cdot\mathbf{Q}$$
$$+\int G_L^o(\mathbf{R}-\mathbf{R}';z,z')\cdot(\mathbf{p}(\mathbf{R}';z')+\mathbf{p}^I(\mathbf{R}';z'))d\mathbf{R}'dz'$$
$$+\int L(\kappa^i;z-z')\cdot\mathcal{P}(z')dz', \quad (49)$$

where for later convenience we have put

$$\mathcal{F}'_{h+}(\kappa)=\mathcal{F}_{h+}+\frac{i\tilde{\omega}^2}{2\varepsilon_0 w_1}(\hat{\mathbf{s}}R_{1N}^s(\kappa)\hat{\mathbf{s}}+\hat{\mathbf{p}}_{1+}R_{1N}^p(\kappa)\hat{\mathbf{p}}_{1-})\cdot\mathbf{Q},$$
$$\mathcal{F}'_{h-}(\kappa)=\mathcal{F}_{h-}, \quad (50)$$

with $\mathbf{Q}$ given by Eq. (18); $G_s(\kappa^i)$ contains contributions from both the transverse and longitudinal fields,

$$G_S(\kappa)=G_T^o(\kappa)+\frac{\kappa}{2\varepsilon_0\varepsilon_1}(\hat{\mathbf{z}}\hat{\mathbf{z}}-\hat{\kappa}\hat{\kappa})$$
$$=\frac{1}{2\varepsilon_0}\left[\frac{i\tilde{\omega}^2}{w_1}\hat{\mathbf{s}}\hat{\mathbf{s}}+\frac{i\kappa^2}{\varepsilon_1 w_1}\hat{\mathbf{z}}\hat{\mathbf{z}}+\frac{iw_1}{\varepsilon_1}\hat{\kappa}\hat{\kappa}\right], \quad (51)$$

where $G_T^o(\kappa)$ is given by Eq. (C7) of Appendix C, and

$$L(\kappa;z-z')\equiv\frac{\kappa}{2\varepsilon_0\varepsilon_1}(\hat{\mathbf{z}}\hat{\mathbf{z}}-\hat{\kappa}\hat{\kappa}-i\hat{\mathbf{z}}\hat{\kappa}-i\hat{\kappa}\hat{\mathbf{z}})\left[\theta(z-z')-\frac{1}{2}\right]$$
$$+\frac{\kappa}{2\varepsilon_0\varepsilon_1}(\hat{\mathbf{z}}\hat{\mathbf{z}}-\hat{\kappa}\hat{\kappa}+i\hat{\mathbf{z}}\hat{\kappa}+i\hat{\kappa}\hat{\mathbf{z}})\left[\theta(z'-z)-\frac{1}{2}\right]. \quad (52)$$

E. Calculational Strategy

At this point we can use κ in place of κ^i, since we have reduced the equations to a form where that is the only wave vector appearing. Combining Eqs. (8) and (49), we have reduced our integral equation to

$$\mathbf{p}(\mathbf{R};z)=\epsilon_0\chi(\mathbf{R};z)\mathbf{F}(\mathbf{R};z) \quad (53)$$

with

$$\mathbf{F}(\mathbf{R};z)=\mathcal{F}+\int G_L^o(\mathbf{R}-\mathbf{R}';z,z')\cdot(\mathbf{p}(\mathbf{R}';z')$$
$$+\mathbf{p}^I(\mathbf{R}';z'))d\mathbf{R}'dz'+\int L(\kappa;z-z')\cdot\mathcal{P}(z')dz', \quad (54)$$

where

$$\mathcal{F}\equiv\mathcal{F}'_{h+}(\kappa)+\mathcal{F}'_{h-}(\kappa)+G_S(\kappa)\cdot\mathbf{Q} \quad (55)$$

with $\mathcal{P}(z)$ and $\mathbf{Q}$ given by Eqs. (16) and (18), with $L(\kappa;z-z')$, $G_L^o(\mathbf{R}-\mathbf{R}';z,z')$, and $G_S(\kappa)$ given, respectively, by Eqs. (52), (A2), and (51). Both because $\mathcal{F}$ is a uniform field and because the other terms in Eq. (54) describe purely longitudinal contributions to the field driving the polarization $\mathbf{p}(\mathbf{R};z)$, it is convenient to imagine that we solve Eqs. (53) and (54) for

an imagined fixed $\mathcal{F}$; the only frequency dependence in this solution arises due to the frequency dependence of $\chi(\mathbf{R};z)$. This then is purely an electrostatic problem. Once $\mathbf{p}(\mathbf{R};z)$ is found in terms of $\mathcal{F}$, then $\mathbf{Q}$ can be written in terms of $\mathcal{F}$ using Eq. (18):

$$\mathbf{Q} = \int W(\mathbf{R}-\mathbf{R}')\mathbf{p}(\mathbf{R}';z')dz'\mathrm{d}\mathbf{R}'. \tag{56}$$

Within our approximations this will be independent of $\mathbf{R}$, of course; it will also be linearly proportional to the effective vector field $\mathcal{F}$, and we write the result as

$$\mathbf{Q} = 4\pi\varepsilon_0\Lambda\cdot\mathcal{F} \tag{57}$$

defining the tensor Λ, which has units of length. In the following subsection we show that once the tensor Λ is determined, the optical properties of the full structure shown in Fig. 1 follow almost immediately. Before doing this, however, we consider further possible simplifications in Eqs. (53)–(55).

We being by focusing on the inclusion of the term $G_S(\kappa)\cdot\mathbf{Q}$ in Eq. (55). At first sight it might seem that this term could be dropped. After all, for κ such that $\tilde{\omega}$, κ, and w_1 are all roughly of the same size, this term is of order $(\tilde{\omega}d)\mathcal{P}/\varepsilon_0$, where $\mathcal{P}$ is a typical value of $\mathcal{P}(z)$, and in the limit $\tilde{\omega}d \ll 1$ this could be considered negligible compared to the rest of $\mathbf{F}(\mathbf{R};z)$ in Eq. (54). However, there are two strong reasons for keeping this term.

First, note that the remaining terms in $\mathbf{F}(\mathbf{R};z)$ include $\mathcal{F}'_{h+}+\mathcal{F}'_{h-}$ as well as contributions from the longitudinal field from $\mathbf{p}(\mathbf{R};z')$; thus both $G_L^o(\mathbf{R}-\mathbf{R}';z,z')$ and $L(\kappa;z-z')$ are purely real, and unless there is any absorption in medium 2, if $G_S(\kappa)\cdot\mathbf{Q}$ were neglected in Eq. (54), we could expect that $\mathbf{Q}$ would be purely in phase with $\mathcal{F}'_{h+}+\mathcal{F}'_{h-}$ (that is, proportional to it with either a positive or negative sign). In the absence of absorption in medium 2, then, we expect that that full Λ of Eq. (57) will be purely real. Then for $\kappa < \tilde{\omega}n_1$ we see that the inclusion of the $G_S(\kappa)\cdot\mathbf{Q}$ term in Eq. (54), and thus in Eq. (57), leads to a component of $\mathbf{Q}$ that is out of phase with $\mathcal{F}'_{h+}+\mathcal{F}'_{h-}$, arising from the transverse field component of $G_S(\kappa)$. This out-of-phase component is a radiation reaction term; it is qualitatively different from the other terms in Eq. (54), is associated with maintaining energy conservation in the entire system, and thus must be kept.

Second, note that if $\kappa \approx \tilde{\omega}n_1$ then $|w_1|/\tilde{\omega} \ll 1$, and the s- and z-components of $G_S(\kappa)\cdot\mathbf{Q}$ can be larger in magnitude than if $\tilde{\omega}$, κ, and w_1 were all roughly of the same size, and thus even if $\kappa > \tilde{\omega}n_1$ and the components of $G_S(\kappa)$ are all real, the contribution of $G_S(\kappa)\cdot\mathbf{Q}$ can be substantial compared to $\mathcal{F}'_{h+}+\mathcal{F}'_{h-}$, and thus should be kept. Note again that this arises from the transverse field component of $G_S(\kappa)$.

In this context, consider now the term involving $L(\kappa;z-z')$ in Eq. (54). As part of the longitudinal field response function, it is purely real and can be expected to be of order $\kappa l \ll 1$ times the corresponding contribution from the term involving $G_L^o(\mathbf{R}-\mathbf{R}';z,z')$. Since there is no qualitative difference characterized by a phase difference between the contributions involving $L(\kappa;z-z')$ and $G_L^o(\mathbf{R}-\mathbf{R}';z,z')$, and since there is no denominator in $L(\kappa;z-z')$ involving w_1 or another such term that diverges as particular values of κ, there is a good argument for neglecting the term involving $L(\kappa;z-z')$ in Eq. (54), and this we do.

It could then be argued that if the term involving $L(\kappa;z-z')$ is neglected, then the longitudinal field contribution to $G_S(\kappa)\cdot\mathbf{Q}$ should be neglected as well, for the same reasons. Nonetheless, we keep this latter term for two reasons. The first is that including it does no harm, and in fact simplifies the form of some of the later equations that arise here. The second, and more important, reason is that by pulling out part of the contribution from the longitudinal field and combining it with $G_T^o(\kappa)$ to form $G_S(\kappa)$, the remaining contribution identified by $L(\kappa;z-z')$ can be shown to not just be small but actually vanish in some special cases. Two of them are, in fact, cases we consider below. One such case is in models where $\chi(\mathbf{R};z)$ is taken to vanish only at a particular $z=z_o$. Then the resulting $\mathbf{p}(\mathbf{R};z)$ [Eq. (53)] vanishes except at $z=z_o$, and in determining Λ we only need $L(\kappa;z-z'=0)$; this vanishes using the limiting expression $\theta(0)=1/2$. A second case is when $\mathcal{P}(z)$ can be assumed to be approximately uniform over the selvedge region; then it is easy to see that the contribution from $L(\kappa;z-z')$ makes no contribution to $\mathbf{Q}$, since

$$\int_0^d \mathrm{d}z\int_0^d \mathrm{d}z' L(\kappa;z-z') = 0.$$

So for increased accuracy in such cases, and for simplicity of the final formulas in all cases, we will construct Λ by neglecting $L(\kappa;z-z')$.

In concluding this subsection we can then summarize our strategy. We solve Eq. (53),

$$\mathbf{p}(\mathbf{R};z) = \varepsilon_0\chi(\mathbf{R};z)\mathbf{F}(\mathbf{R};z), \tag{58}$$

for the polarization $\mathbf{p}(\mathbf{R};z)$ in terms of $\mathcal{F}$, where

$$\mathbf{F}(\mathbf{R};z) = \mathcal{F} + \int G_L^o(\mathbf{R}-\mathbf{R}';z,z') \cdot(\mathbf{p}(\mathbf{R}';z') + \mathbf{p}^I(\mathbf{R}';z'))d\mathbf{R}'\mathrm{d}z' \tag{59}$$

[Eq. (54) with the neglect of $L(\kappa;z-z')$]. Here $G_L^o(\mathbf{R}-\mathbf{R}';z,z')$ is the electrostatic Green function [Eq. (A2)], and $\mathbf{p}^I(\mathbf{R};z)$ is the (electrostatic) image polarization [Eq. (43)] in the layer beneath the cladding. We then construct a coarse-grained polarization $\mathcal{P}(z)$ [Eq. (16)] and determine its integral over z, $\mathbf{Q}$ [Eq. (56)]. Finally, we extract the tensor Λ according to Eq. (57). We stress that what is involved in these calculations is only electrostatic fields. The inclusion of retardation arises here through the transverse part of the electric field, which is included as part of $\mathcal{F}$ but need not be identified explicitly at this point. Its effects will arise in the full solution for the field everywhere, to which we now turn.

F. Transfer Matrices

Returning to Fig. 1, and considering first the bare multilayer structure without a selvedge, the natural way to treat its optical properties is to introduce transfer matrices that connect the upward- and downward-propagating (or evanescent) fields in different parts of the structure. For the method for doing this that we will adopt later in the paper, see [31]. With the presence of the selvedge, an obvious strategy is to introduce an additional transfer matrix for the selvedge region; it can then be combined with the other transfer matrices describing the other features of the system to allow for an easy calculation of the optical response. Since it is only the coarse-grained fields that will lead to fields far from the structure [see discussion after Eq. (20)], we only need to deal with coarse-grained fields in the transfer matrix treatment. To do this, we imagine

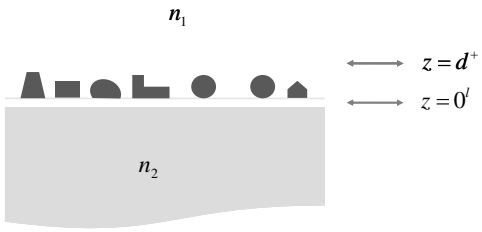

Fig. 3. Inserting an infinitesimal layer of cladding beneath the selvedge and above the multilayer. This allows us to work with only coarse-grained fields in the transfer-matrix treatment.

inserting an infinitesimal layer of medium 1 just above the material of relative permittivity ε_2, and just below the lowest extent of the NPs, that is, just below the lowest part of the selvedge (see Fig. 3). We label the position of this layer $z = 0^l$, and we want to relate the coarse-grained field $\bar{\mathbf{E}}(\mathbf{R}, z)$ at $z = 0^l$ to the coarse-grained field at $z = d^+$ in medium 1 just above the highest extent of the NPs, that is, just over the top of the selvedge.

In Appendix D we show that the coarse-grained field at these two positions can be written as

$$\begin{aligned}\bar{\mathbf{E}}(\mathbf{R}; d^+) &= \bar{\mathbf{E}}^+(d^+)e^{i\kappa\cdot\mathbf{R}} + \bar{\mathbf{E}}^-(d^+)e^{i\kappa\cdot\mathbf{R}},\\ \bar{\mathbf{E}}(\mathbf{R}; 0^l) &= \bar{\mathbf{E}}^+(0^l)e^{i\kappa\cdot\mathbf{R}} + \bar{\mathbf{E}}^-(0^l)e^{i\kappa\cdot\mathbf{R}},\end{aligned} \tag{60}$$

where the superscripts + indicate the components of upward-propagating (or evanescent) waves, and the superscripts – indicate the components of downward-propagating (or evanescent) waves, with

$$\begin{aligned}\bar{\mathbf{E}}^+(d^+) &= \mathcal{F}'_{h+}(\kappa) + \frac{i\tilde{\omega}^2}{2\varepsilon_0 w_1}(\hat{\mathbf{s}}\hat{\mathbf{s}} + \hat{\mathbf{p}}_{1+}\hat{\mathbf{p}}_{1+})\cdot\mathbf{Q},\\ \bar{\mathbf{E}}^-(d^+) &= \mathcal{F}'_{h-}(\kappa),\\ \bar{\mathbf{E}}^+(0^l) &= \mathcal{F}'_{h+}(\kappa),\\ \bar{\mathbf{E}}^-(0^l) &= \mathcal{F}'_{h-}(\kappa) + \frac{i\tilde{\omega}^2}{2\varepsilon_0 w_1}(\hat{\mathbf{s}}\hat{\mathbf{s}} + \hat{\mathbf{p}}_{1-}\hat{\mathbf{p}}_{1-})\cdot\mathbf{Q}.\end{aligned} \tag{61}$$

From these equations we can write

$$\begin{aligned}\bar{\mathbf{E}}^+(d^+) &= \bar{\mathbf{E}}^+(0^l) + \frac{i\tilde{\omega}^2}{2\varepsilon_0 w_1}(\hat{\mathbf{s}}\hat{\mathbf{s}} + \hat{\mathbf{p}}_{1+}\hat{\mathbf{p}}_{1+})\cdot\mathbf{Q},\\ \bar{\mathbf{E}}^-(d^+) &= \bar{\mathbf{E}}^-(0^l) - \frac{i\tilde{\omega}^2}{2\varepsilon_0 w_1}(\hat{\mathbf{s}}\hat{\mathbf{s}} + \hat{\mathbf{p}}_{1-}\hat{\mathbf{p}}_{1-})\cdot\mathbf{Q},\end{aligned} \tag{62}$$

and now writing $\mathbf{Q}$ in terms of $\bar{\mathbf{E}}^+(0^l)$ and $\bar{\mathbf{E}}^-(0^l)$ will let us construct our transfer matrices. Combining Eqs. (57) and (61), we find

$$\mathbf{Q} = 4\pi\varepsilon_0\Lambda\cdot\left(\bar{\mathbf{E}}^+(0^l) + \bar{\mathbf{E}}^-(0^l) - \frac{i\kappa}{2\varepsilon_0\varepsilon_1}(\hat{\mathbf{z}}\hat{\kappa} + \hat{\kappa}\hat{\mathbf{z}})\cdot\mathbf{Q}\right), \tag{63}$$

where we have used Eq. (55) and (50) for $\mathcal{F}$, and Eq. (51) for $G_S(\kappa)$.

For simplicity we now assume that, at least for our κ of choice, Λ can be written in the form

$$\Lambda = \Lambda_s\hat{\mathbf{s}}\hat{\mathbf{s}} + \Lambda_\kappa\hat{\kappa}\hat{\kappa} + \Lambda_z\hat{\mathbf{z}}\hat{\mathbf{z}}. \tag{64}$$

This is not unreasonable given the form of Eqs. (58) and (59). At least for random or reasonably symmetric $\chi(\mathbf{R}; z)$, we would in fact expect $\Lambda = \Lambda_\parallel(\hat{\mathbf{x}}\hat{\mathbf{x}} + \hat{\mathbf{y}}\hat{\mathbf{y}}) + \Lambda_\perp\hat{\mathbf{z}}\hat{\mathbf{z}}$, which, since $\hat{\mathbf{x}}\hat{\mathbf{x}} + \hat{\mathbf{y}}\hat{\mathbf{y}} = \hat{\kappa}\hat{\kappa} + \hat{\mathbf{s}}\hat{\mathbf{s}}$ for any $\hat{\kappa}$, guarantees that we indeed have Eq. (64) with $\Lambda_s = \Lambda_\kappa$. However, we only assume the slightly weaker Eq. (64) here. This will guarantee that there is no mixing of *s*- and *p*-polarized light, and we can consider these two polarizations separately; a generalization of this is complicated but straightforward.

1. s-Polarized Light

First consider *s*-polarized light, for which we have $\bar{\mathbf{E}}^+(d^+) = \hat{s}\bar{E}^+(d^+)$, and similarly for all the other electric field terms in Eq. (62). Then seeking a $\mathbf{Q} = Q_s\hat{\mathbf{s}}$, from Eq. (63) we have

$$Q_s = 4\pi\varepsilon_0\Lambda_s(\bar{E}^+(0^l) + \bar{E}^-(0^l)),$$

and seeking a solution $\bar{\mathbf{E}}^+(d^+) = \hat{s}\bar{E}^+(d^+)$, etc., in Eq. (62) we find

$$\begin{aligned}\bar{E}^+(d^+) &= (1 + n_{os})\bar{E}^+(0^l) + n_{os}\bar{E}^-(0^l),\\ \bar{E}^-(d^+) &= -n_{os}\bar{E}^+(0^l) + (1 - n_{os})\bar{E}^-(0^l),\end{aligned}$$

where

$$n_{os} \equiv \frac{2\pi i\tilde{\omega}^2}{w_1}\Lambda_s. \tag{65}$$

That is,

$$\begin{bmatrix}\bar{E}^+(d^+)\\ \bar{E}^-(d^+)\end{bmatrix} = m_s\begin{bmatrix}\bar{E}^+(0^l)\\ \bar{E}^-(0^l)\end{bmatrix},$$

where the transfer matrix for the NP region is

$$m_s = \begin{bmatrix}1 + n_{os} & n_{os}\\ -n_{os} & 1 - n_{os}\end{bmatrix}. \tag{66}$$

2. p-Polarized Light

For *p*-polarized light the situation is more complicated; here $\bar{\mathbf{E}}^+(0^l)$ and $\bar{\mathbf{E}}^-(0^l)$ point in different directions [recall Eq. (39)],

$$\begin{aligned}\bar{\mathbf{E}}^+(0^l) &= \bar{E}^+(0^l)\hat{\mathbf{p}}_{1+},\\ \bar{\mathbf{E}}^-(0^l) &= \bar{E}^-(0^l)\hat{\mathbf{p}}_{1-},\end{aligned} \tag{67}$$

and similarly

$$\begin{aligned}\bar{\mathbf{E}}^+(d^+) &= \bar{E}^+(d^+)\hat{\mathbf{p}}_{1+},\\ \bar{\mathbf{E}}^-(d^+) &= \bar{E}^-(d^+)\hat{\mathbf{p}}_{1-}.\end{aligned} \tag{68}$$

Using Eq. (67) in Eq. (63), and recalling Eq. (64), we can solve for Q_κ and Q_z. Using the results in Eq. (62) we find, after some algebra,

$$\begin{aligned}&\bar{E}^+(d^+)\\ &= \bar{E}^+(0^l) + \frac{(n_{oz} - n_{o\kappa})\bar{E}^-(0^l) + (n_{oz} + n_{o\kappa} + 2n_{oz}n_{o\kappa})\bar{E}^+(0^l)}{1 - n_{oz}n_{o\kappa}},\\ &\bar{E}^-(d^+)\\ &= \bar{E}^-(0^l) - \frac{(n_{oz} + n_{o\kappa} - 2n_{oz}n_{o\kappa})\bar{E}^-(0^l) + (n_{oz} - n_{o\kappa})\bar{E}^+(0^l)}{1 - n_{oz}n_{o\kappa}},\end{aligned} \tag{69}$$

where

$$n_{oz} \equiv \frac{2\pi i\kappa^2}{\varepsilon_1 w_1}\Lambda_z,$$
$$n_{o\kappa} \equiv \frac{2\pi i w_1}{\varepsilon_1}\Lambda_\kappa. \tag{70}$$

Now the quantities n_{oz} and $n_{o\kappa}$ will contain factors of order $\tilde{\omega}d$. Nonetheless, n_{os} and $n_{o\kappa}$ can be large because, depending on the value of κ, it is possible for $|w_1| \ll \tilde{\omega}, \kappa$. So we cannot naively assume that these quantities are small [see discussion following Eq. (57)]. However, the product $n_{oz}n_{o\kappa}$ that appears in Eq. (69) has no factor of w_1 in the denominator; using Eq. (70) we find

$$n_{oz}n_{o\kappa} = -\frac{4\pi^2\kappa^2\Lambda_z\Lambda_\kappa}{\varepsilon_1^2}.$$

With no dangerous w_1 term in the denominator we can neglect this term quadratic in $\tilde{\omega}d$, and then Eq. (69) reduces to

$$\bar{E}^+(d^+) = \bar{E}^+(0^l) + n_-\bar{E}^-(0^l) + n_+\bar{E}^+(0^l),$$
$$\bar{E}^-(d^+) = \bar{E}^-(0^l) - n_+\bar{E}^-(0^l) - n_-\bar{E}^+(0^l),$$

where we have defined

$$n_\pm \equiv n_{oz} \pm n_{o\kappa}, \tag{71}$$

or

$$\begin{bmatrix}\bar{E}^+(d^+)\\ \bar{E}^-(d^+)\end{bmatrix} = m_p'\begin{bmatrix}\bar{E}^+(0^l)\\ \bar{E}^-(0^l)\end{bmatrix},$$

where the transfer matrix is

$$m_p' = \begin{bmatrix}1+n_+ & n_-\\ -n_- & 1-n_+\end{bmatrix}, \tag{72}$$

and we use a "prime" here because we will introduce a different version of this below.

3. Selvedge Fresnel Coefficients

Our main interest in this paper is how the presence of the selvedge affects any resonances associated with the multilayer structure below, such as WG modes. However, it is also interesting to characterize the selvedge region by its own Fresnel coefficients, because they will be seen to be an important component of the whole system of bulk and selvedge. We note that the "isolated" selvedge we consider here, bounded above and below by media of relative permittivity ε_1, is a formal structure that can be taken as defined by the transfer matrices [Eqs. (66), (72)]. It should not be thought of as a region of material physically bounded on either side by a medium of relative permittivity ε_1, because the effect of the image charges that depend on the medium that is *actually* below the selvedge in our real structure of interest appears in Λ, and thus in n_{os}, $n_{o\kappa}$, and n_{oz}.

In general a transfer matrix identified with a structure takes the form [31]

$$m = \begin{bmatrix}\frac{T_{+-}T_{-+}-R_{+-}R_{-+}}{T_{+-}} & \frac{R_{+-}}{T_{+-}}\\ -\frac{R_{-+}}{T_{+-}} & \frac{1}{T_{+-}}\end{bmatrix}, \tag{73}$$

where T_{+-} is the transmission coefficient for light incident from above, R_{-+} is the reflection coefficient for light incident from below, etc. For *s*-polarized light we can use Eq. (66) to identify

$$T_{+-} = T_{-+} = \frac{1}{1-n_{os}} \equiv t_s, \tag{74}$$

$$R_{+-} = R_{-+} = \frac{n_{os}}{1-n_{os}} \equiv r_s, \tag{75}$$

and in this notation we can write the transfer matrix [Eq. (66)] of the selvedge for *s*-polarized light as

$$m_s = \begin{bmatrix}\frac{t_s^2-r_s^2}{t_s} & \frac{r_s}{t_s}\\ -\frac{r_s}{t_s} & \frac{1}{t_s}\end{bmatrix}.$$

For *p*-polarized light the situation is again more complicated. We can use Eqs. (72) and (73) to identify

$$R_{+-} = R_{-+} = \frac{n_-}{1-n_+},$$
$$T_{+-} = \frac{1}{1-n_+},$$
$$T_{-+} = \frac{1-4n_{oz}n_{o\kappa}}{1-n_+}.$$

However, we have already made and justified the approximation of neglecting terms of order $n_{oz}n_{o\kappa}$, so we take

$$T_{-+} \to \frac{1}{1-n_+}$$

within our approximations as well. If we now put

$$T_{+-} = T_{-+} = \frac{1}{1-n_+} \equiv t_p, \tag{76}$$

$$R_{+-} = R_{-+} = \frac{n_-}{1-n_+} \equiv r_p, \tag{77}$$

and construct the matrix

$$m_p \equiv \begin{bmatrix}\frac{t_p^2-r_p^2}{t_p} & \frac{r_p}{t_p}\\ -\frac{r_p}{t_p} & \frac{1}{t_p}\end{bmatrix},$$

we have

$$m_p = \begin{bmatrix}\frac{1-n_-^2}{1-n_+} & n_-\\ -n_- & 1-n_+\end{bmatrix}. \tag{78}$$

This is different from the m_p' of Eq. (72), since $(1-n_-^2)/(1-n_+) \neq (1+n_+)$; however, it differs from it only by terms of order $n_{oz}n_{o\kappa}$, and so within our approximations indeed m_p' and m_p are in fact equivalent. It will be more convenient to use m_p.

G. Optical Response and System Resonances

The full transfer matrix for the entire system (see Fig. 1) is then

$$\begin{bmatrix} \frac{T'_{1N}T'_{1N}-R'_{1N}R'_{1N}}{T'_{1N}} & \frac{R'_{1N}}{T'_{1N}} \\ -\frac{R'_{1N}}{T'_{1N}} & \frac{1}{T'_{1N}} \end{bmatrix} = \begin{bmatrix} \frac{t^2-r^2}{t} & \frac{r}{t} \\ -\frac{r}{t} & \frac{1}{t} \end{bmatrix} \begin{bmatrix} \frac{T_{1N}T_{N1}-R_{1N}R_{N1}}{T_{1N}} & \frac{R_{1N}}{T_{1N}} \\ -\frac{R_{N1}}{T_{1N}} & \frac{1}{T_{1N}} \end{bmatrix}, \tag{79}$$

where t and r are either t_s and r_s or t_p and r_p, depending on whether we are dealing with s or p polarization; similarly T_{1N} is the transmission Fresnel coefficient from region 1 to region N, before any selvedge is included, for s- or p-polarized light as appropriate, and likewise for the other such coefficients; and T'_{1N} is the full transmission Fresnel coefficient from region 1 to region N when we include the selvedge. With a bit of algebra we find from Eq. (79) that

$$\begin{aligned} T'_{1N} &= \frac{tT_{1N}}{1-rR_{1N}}, \\ R'_{1N} &= r + \frac{tR_{1N}t}{1-rR_{1N}}, \\ R'_{1N} &= R_{N1} + \frac{T_{N1}rT_{1N}}{1-rR_{1N}}, \\ T'_{1N} &= \frac{T_{N1}t}{1-rR_{1N}}. \end{aligned} \tag{80}$$

Note that Eq. (80) follows exactly from Eq. (79), and the physics of the combination of Fresnel coefficients is apparent. These results can be used to describe the full optical properties of the system, in particular its response to incident fields. We defer this discussion to a later publication and focus here on how a WG (or similar) resonance is slightly shifted by the presence of the selvedge.

For κ near a WG (or similar) resonance at κ_o of the bare multilayer structure, we will generally have a divergence in the Fresnel coefficients T_{1N}, T_{N1}, R_{1N}, and R_{N1}. These poles in the Fresnel coefficients signal the presence of the electromagnetic excitation bound to the multilayer structure, for such field structures propagate in the xy plane and have fields evanescent in both the cladding and the substrate; thus, for example, R_{1N} must diverge because it gives the ratio of the upward evanescent field to the downward evanescent field, and at a resonance κ_o there can be an upward evanescent field in the cladding without any downward evanescent field. We work out the resonance structure of the Fresnel coefficients in Appendix E for a simple WG structure, which will serve as an example in calculations later in this paper, but even more generally we can expect that for κ close to κ_o we have the behavior

$$\begin{aligned} T_{1N} &\approx \frac{\tau_{1N}}{\kappa-\kappa_o}, \\ T_{N1} &\approx \frac{\tau_{N1}}{\kappa-\kappa_o}, \\ R_{1N} &\approx \frac{\rho_{1N}}{\kappa-\kappa_o}, \\ R_{N1} &\approx \frac{\rho_{N1}}{\kappa-\kappa_o}, \end{aligned} \tag{81}$$

where τ_{1N}, τ_{N1}, ρ_{1N} and ρ_{N1} are constants that depend on the structure and on the excitation resonance κ_o (if there is more than one). Writing down the product of interface and propagation transfer matrices that determines the transfer matrix of the bare multilayer, and noting that by inspection we find the elements of all these matrices are zero or finite, we see that the full transfer matrix of the bare multilayer [the rightmost matrix on the right-hand side of Eq. (79)] has terms that must be all finite or zero. Substituting the near-resonance behavior [Eq. (81)] into that transfer matrix, we then see that

$$\tau_{1N}\tau_{N1} - \rho_{1N}\rho_{N1} = 0,$$

and further that

$$\frac{T_{1N}T_{N1} - R_{1N}R_{N1}}{T_{1N}} \equiv \Gamma_{1N}$$

is finite at all κ. Note that we can write the third term of Eq. (80) as

$$R'_{N1} = \frac{R_{N1} + r\Gamma_{1N}T_{1N}}{1-rR_{1N}}.$$

Then using Eq. (81) in this and the expressions for T'_{1N}, R'_{1N}, and T'_{1N} in Eq. (80), we have

$$\begin{aligned} T'_{N1} &= \frac{t\tau_{1N}}{\kappa-\kappa_o-r\rho_{1N}}, \\ R'_{N1} &= r + \frac{t\rho_{1N}t}{\kappa-\kappa_o-r\rho_{1N}}, \\ R'_{N1} &= \frac{\rho_{N1} + r\Gamma_{1N}\tau_{1N}}{\kappa-\kappa_o-r\rho_{1N}}, \\ T'_{N1} &= \frac{\tau_{N1}t}{\kappa-\kappa_o-r\rho_{1N}}, \end{aligned} \tag{82}$$

where to at least first approximation we can evaluate r and t at κ_o. The new resonance is at $\kappa = \kappa'_0$, where

$$\kappa'_0 = \kappa_o + r\rho_{1N}. \tag{83}$$

The shift $r\rho_{1N}$ will in general have both real an imaginary parts, indicating both a shift in the position of the resonance and a broadening of it due to absorption in the selvedge. We turn to these matters below.

3. TOY MODELS

In summary, then, for a given selvedge and WG structure the Fresnel coefficients [Eq. (82)] that characterize the optical properties of the structure are determined by solving the selvedge equations [Eqs. (57)–(59)] to determine the matrix Λ, using that to determine the transfer matrix coefficients n_{os}, $n_{o\kappa}$, and n_{oz}, according to Eqs. (65) and (70) for simple selvedges [Eq. (64)], and then constructing the selvedge Fresnel coefficients r and t according to Eqs. (74)–(77). The first of these tasks will typically require a numerical solution, but only of equations of electrostatics and only involving the cladding dielectric constant and that of the material immediately below it in the bare multilayer structure.

To illustrate this strategy, we address in this section the first of these tasks for three simple "toy models" that allow analytic solutions. We stress that our approach is not limited to such simple models, and indeed its main application will certainly be to more realistic selvedge models where numerical solutions of Eqs. (57)–(59) for Λ can be performed. However, the toy models we consider here are interesting

in their own right and will be useful comparisons for the more realistic models to which we plan to turn in future publications.

A. Lattice of Spheres in the Point Dipole Approximation

See Fig. 4(a). Here we assume that the $\chi(\mathbf{R},z)$ of (53) takes the form

$$\chi(\mathbf{R},z)=\sum_{\alpha}\chi^{(\alpha)}(\mathbf{R},z),$$

where

$$\chi^{(\alpha)}(\mathbf{R},z)=(\varepsilon-\varepsilon_1)\theta(b-|\mathbf{r}-\mathbf{r}^{(\alpha)}|),$$

where $\mathbf{r}^{(\alpha)}=\mathbf{R}^{(\alpha)}+\hat{\mathbf{z}}h$ labels the position of the αth sphere. The spheres are all taken to have a relative permittivity ε, and to be of radius b, with their centers at a distance h above the interface with the first material below the cladding; we take $b\le h$, and also b is less than the distance between the sites $\mathbf{R}^{(\alpha)}$ of the two dimensional lattice. Similarly, with

$$\mathbf{p}(\mathbf{R},z)=\sum_{\alpha}\mathbf{p}^{(\alpha)}(\mathbf{R},z), \tag{84}$$

where each $\mathbf{p}^{(\alpha)}(\mathbf{R},z)$ is nonzero only where the corresponding $\chi^{(\alpha)}(\mathbf{R},z)$ is nonzero, we will consider an approximate solution when the polarization in the spheres is uniform and, with respect to their interaction with each other and the layers, they can be taken as point dipoles. That is, we seek a solution

$$\mathbf{p}^{(\alpha)}(\mathbf{R},z)\simeq\frac{3\mu}{4\pi b^3}\theta(b-|\mathbf{r}-\mathbf{r}^{(\alpha)}|), \tag{85}$$

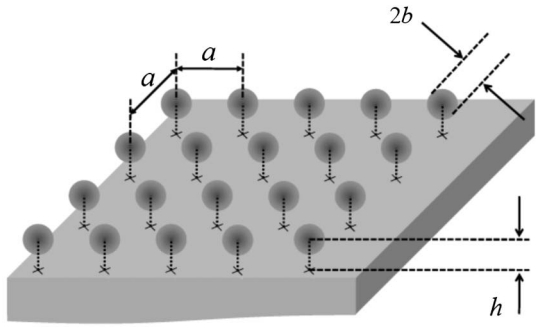

(a)

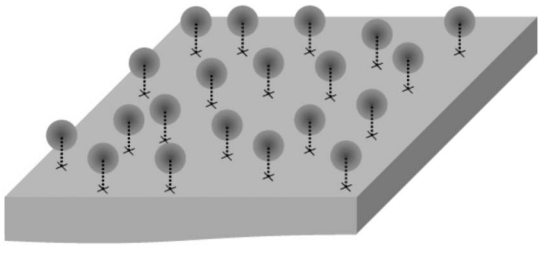

(b)

Fig. 4. (a) Square lattice of spherical NPs of radius $b$with lattice spacing a at a height h above the substrate; (b) a disordered arrangement of spherical NPs of radius b, with average interparticle spacing a at a height h above the substrate.

where μ is a dipole moment to be determined, which by ansatz will be the same for each α; and for points $\mathbf{R}'$ near sites $\alpha'\neq\alpha$, we assume

$$\mathbf{p}^{(\alpha)}(\mathbf{R}',z')\simeq\mu\delta(\mathbf{R}'-\mathbf{r}^{(\alpha)}) \tag{86}$$

in Eq. (59). Taking $\mathcal{A}$ to be the area of a unit cell in the plane at $z=h$, it then follows from Eqs. (18) and (85) that

$$\mathbf{Q}=\frac{\mu}{\mathcal{A}}. \tag{87}$$

Of course, we obviously cannot use Eq. (86) for points $\mathbf{r}$ in the neighborhood of site α. However, using Eqs. (85) and (A2) and the properties of the electrostatic dipole field,

$$\int G_L^o(\mathbf{R}-\mathbf{R}';z,z')\cdot\mathbf{p}^{(\alpha)}(\mathbf{R}',z')d\mathbf{R}'\mathrm{d}z' = -\frac{\mu}{4\pi\epsilon_0\varepsilon_1 b^3}\quad\text{for } |\mathbf{r}-\mathbf{r}^{(\alpha)}|<b.$$

Adopting Eq. (86) for the other sites when we are at such $\mathbf{r}$, we find

$$\int G_L^o(\mathbf{R}-\mathbf{R}';z,z')\cdot\mathbf{p}^{(\alpha')}(\mathbf{R}',z')d\mathbf{R}'\mathrm{d}z' = G_L^o(\mathbf{R}-\mathbf{R}^{(\alpha')};z,h)\cdot\mu,\quad\text{for } |\mathbf{r}-\mathbf{r}^{(\alpha)}|<b\quad\text{and}\quad\alpha'\neq\alpha.$$

Thus using Eq. (84), we have

$$\int G_L^o(\mathbf{R}-\mathbf{R}';z,z')\cdot\mathbf{p}(\mathbf{R}',z')d\mathbf{R}'\mathrm{d}z' = -\frac{\mu}{4\pi\epsilon_0\varepsilon_1 b^3}+\sum_{\alpha'\neq\alpha}G_L^o(\mathbf{R}-\mathbf{R}^{(\alpha')};z,h)\cdot\mu,\quad\text{for } |\mathbf{r}-\mathbf{r}^{(\alpha)}|<b. \tag{88}$$

This is one of the terms we need on the right-hand side of Eq. (59). The other term involves the image polarization. Defining

$$M\equiv\frac{\varepsilon_2-\varepsilon_1}{\varepsilon_2+\varepsilon_1}(\hat{\mathbf{z}}\,\hat{\mathbf{z}}-\hat{\mathbf{x}}\,\hat{\mathbf{x}}-\hat{\mathbf{y}}\,\hat{\mathbf{y}}),$$

from Eq. (45) we can write

$$\mathbf{p}^I(\mathbf{R},z)=M\cdot\mathbf{p}(\mathbf{R},-z).$$

Since we will never need the field where the image dipoles are, a first approximation for this would be to use Eq. (86) and find

$$\mathbf{p}^I(\mathbf{R},z)=M\cdot\sum_{\alpha'}\mu\delta(\mathbf{R}-\mathbf{R}^{(\alpha')})\delta(z+h).$$

Using this in Eq. (59), together with Eq. (88), we find

$$\mathbf{F}(\mathbf{R};z)=\mathcal{F}-\frac{\mu}{4\pi\epsilon_0\varepsilon_1 b^3}+\sum_{\alpha'\neq\alpha}G_L^o(\mathbf{R}-\mathbf{R}^{(\alpha')};z,h)\cdot\mu+\sum_{\alpha'}G_L^o(\mathbf{R}-\mathbf{R}^{(\alpha')};z,-h)\cdot M\cdot\mu,\quad\text{for } |\mathbf{r}-\mathbf{r}^{(\alpha)}|<b. \tag{89}$$

We can use this expression now in determining $\mathbf{p}^{(\alpha)}(\mathbf{R},z)$, since for $|\mathbf{r}-\mathbf{r}^{(\alpha)}|<b$ we have [from Eq. (53)]

$$\mathbf{p}^{(\alpha)}(\mathbf{R},z)=\epsilon_0\chi^{(\alpha)}(\mathbf{R},z)\mathbf{F}(\mathbf{R};z)$$

For such points we make the point dipole approximation by putting $\mathbf{F}(\mathbf{R};z)\simeq\mathbf{F}(\mathbf{R}^{(\alpha)};h)$ and then integrating over the sphere to find [see Eq. (85)]

$$\begin{aligned}\frac{\mu}{\frac{4\pi}{3}b^3\epsilon_0(\varepsilon-\varepsilon_1)}&=\mathcal{F}-\frac{\mu}{4\pi\epsilon_0\varepsilon_1 b^3}\\&+\sum_{\alpha'\neq\alpha}G_L^o(\mathbf{R}^{(\alpha)}-\mathbf{R}^{(\alpha')};h,h)\cdot\mu\\&+\sum_{\alpha'}G_L^o(\mathbf{R}^{(\alpha)}-\mathbf{R}^{(\alpha')};h,-h)\cdot M\cdot\mu.\end{aligned}\tag{90}$$

Bringing the second term on the right-hand side of Eq. (90) over to the left-hand side and rewriting the result, we have

$$\begin{aligned}\frac{\mu}{\frac{4\pi}{3}b^3\epsilon_0\left(\frac{3\varepsilon_1(\varepsilon-\varepsilon_1)}{\varepsilon+2\varepsilon_1}\right)}&=\mathcal{F}+\sum_{\alpha'\neq\alpha}G_L^o(\mathbf{R}^{(\alpha)}-\mathbf{R}^{(\alpha')};h,h)\cdot\mu\\&+\sum_{\alpha'}G_L^o(\mathbf{R}^{(\alpha)}-\mathbf{R}^{(\alpha')};h,-h)\cdot M\cdot\mu,\end{aligned}\tag{91}$$

displaying the result in terms of the polarizability of a sphere of relative permittivity ε embedded in a background medium of relative permittivity ε_1. Defining a dimensionless tensor S according to

$$\begin{aligned}S&\equiv 4\pi\epsilon_0\mathcal{A}^{3/2}\sum_{\alpha'\neq\alpha}G_L^o(\mathbf{R}^{(\alpha)}-\mathbf{R}^{(\alpha')};h,h)\\&+4\pi\epsilon_0\mathcal{A}^{3/2}\sum_{\alpha'}G_L^o(\mathbf{R}^{(\alpha)}-\mathbf{R}^{(\alpha')};h,-h)\cdot M\\&=4\pi\epsilon_0\mathcal{A}^{3/2}\sum_{\alpha'\neq 0}G_L^o(-\mathbf{R}^{(\alpha')};h,h)\\&+4\pi\epsilon_0\mathcal{A}^{3/2}\sum_{\alpha'}G_L^o(-\mathbf{R}^{(\alpha')};h,-h)\cdot M,\end{aligned}\tag{92}$$

where the first expression is clearly independent of α, and so in the second we have taken $\mathbf{R}^{(\alpha)}=0$ for ease of evaluation, we can write Eq. (91) as

$$\mathbf{Q}=\left[\frac{\varepsilon_1(\varepsilon-\varepsilon_1)}{\varepsilon+2\varepsilon_1}\frac{b^3}{\mathcal{A}}\right]\left[4\pi\epsilon_0\mathcal{F}+\frac{1}{\mathcal{A}^{1/2}}S\cdot\mathbf{Q}\right],$$

where we have used Eq. (18). We recover the form Eq. (57) by taking

$$\Lambda\equiv\left[\frac{\varepsilon_1(\varepsilon-\varepsilon_1)}{\varepsilon+2\varepsilon_1}\frac{b^3}{\mathcal{A}}\right]\left(U-\frac{\varepsilon_1(\varepsilon-\varepsilon_1)}{\varepsilon+2\varepsilon_1}\frac{b^3}{\mathcal{A}^{3/2}}S\right)^{-1},\tag{93}$$

which is independent of κ. For simple lattices we will have

$$\Lambda=\Lambda_\perp\hat{\mathbf{z}}\hat{\mathbf{z}}+\Lambda_\parallel(\hat{\mathbf{x}}\hat{\mathbf{x}}+\hat{\mathbf{y}}\hat{\mathbf{y}})=\Lambda_\perp\hat{\mathbf{z}}\hat{\mathbf{z}}+\Lambda_\parallel(\hat{\mathbf{s}}\hat{\mathbf{s}}+\hat{\kappa}\hat{\kappa})$$

in which case we can write Eq. (64) with $\Lambda_z=\Lambda_\perp$ and $\Lambda_s=\Lambda_\kappa=\Lambda_\parallel$; $n_{os}, n_{o\kappa}$, and n_{oz} then follow immediately from Eqs. (65) and (70).

B. Disordered Arrangement of Spheres in the Point Dipole Approximation

See Fig. 4(b). Here much of the analysis of the preceding subsection follows through. We take $\mathbf{R}^{(\alpha)}$ to be the positions of the spheres and $\mathcal{A}$ to be defined such that $\mathcal{A}^{-1}$ is the (areal) density of spheres in the surface. The only different part of the derivation required is a mean field approximation for the tensor S. We explicitly keep the image term for the sphere α in the second term of Eq. (92), the term with $\alpha'=\alpha$. Then, since an area $\mathcal{A}$ is on average assigned to each sphere, corresponding to a circle with radius $(\mathcal{A}/\pi)^{1/2}$ in the plane, the simplest mean field approximation is just to replace the sums in Eq. (92) over dipoles $\alpha'\neq\alpha$ by integrals as below:

$$\begin{aligned}S&=4\pi\epsilon_0\mathcal{A}^{3/2}G_L^o(\mathbf{R}=0;h,-h)\cdot M\\&+4\pi\epsilon_0\mathcal{A}^{3/2}\int_{R=(\mathcal{A}/\pi)^{1/2}}^{\infty}\int_{\phi=0}^{2\pi}\frac{d\mathbf{R}}{\mathcal{A}}G_L^o(-\mathbf{R};h,h)\\&+4\pi\epsilon_0\mathcal{A}^{3/2}\int_{R=(\mathcal{A}/\pi)^{1/2}}^{\infty}\int_{\phi=0}^{2\pi}\frac{d\mathbf{R}}{\mathcal{A}}G_L^o(-\mathbf{R};h,-h)\cdot M,\end{aligned}\tag{94}$$

where $\mathbf{R}=(R\cos\phi,R\sin\phi)$, and $d\mathbf{R}=RdRd\phi$. This value of S can then be used in Eq. (93), and the rest of the derivation of the preceding section can be followed to get to Eqs. (65) and (70).

C. Planar Layer

Here we work out a particularly simple case. We take

$$\begin{aligned}&\chi(\mathbf{R},z)=(\varepsilon-\varepsilon_1)\qquad\text{for } 0<z<d,\\&\chi(\mathbf{R},z)=0\qquad\text{otherwise.}\end{aligned}\tag{95}$$

This corresponds to a slab of material on top of our structure with relative permittivity ε. Of course, the optical properties of this structure can be treated exactly, because the addition of this selvedge to our original multilayer structure just makes a more complicated multilayer structure. However, it is useful to treat it within the approximate framework that we are using to help in the comparison of model systems. With Eq. (95) we naturally seek a solution of our approximate equations [Eqs. (53), (55), and (59)] with

$$\mathbf{p}(\mathbf{R},z)=\mathbf{p}(z)=\mathcal{P}(z),\tag{96}$$

where the second inequality follows immediately from Eq. (16). We now look at the terms in Eq. (59). We have

$$\begin{aligned}&\int G_L^o(\mathbf{R}-\mathbf{R}';z,z')\cdot\mathbf{p}(\mathbf{R}',z')d\mathbf{R}'dz'\\&=\int G_L^o(\mathbf{R}-\mathbf{R}';z,z')\cdot\mathbf{p}(z')d\mathbf{R}'dz'\\&=\int G_L^o(\kappa=0;z,z')\cdot\mathbf{p}(z')dz'\\&=-\frac{1}{\epsilon_0\varepsilon_1}\hat{\mathbf{z}}\hat{\mathbf{z}}\cdot\mathbf{p}(z),\qquad\text{for } 0<z<d,\end{aligned}$$

where we have used the indicated limit of Eq. (C3). Similarly,

$$\int G_L^o(\mathbf{R}-\mathbf{R}';z,z')\cdot\mathbf{p}^I(\mathbf{R}',z')d\mathbf{R}'\mathrm{d}z'=0 \quad \text{for } 0<z<d$$

since the image polarization exists outside that region. Using these results together with Eqs. (95) and (96) in Eqs. (53) and (59), we have

$$\mathcal{P}(z)=\epsilon_0(\varepsilon-\varepsilon_1)\left[\mathcal{F}-\frac{1}{\epsilon_0\varepsilon_1}\hat{\mathbf{z}}\hat{\mathbf{z}}\cdot\mathcal{P}(z)\right] \quad \text{for } 0<z<d.$$

Solving for $\mathcal{P}(z)$ and then finding $\mathbf{Q}$ from Eq. (18) yields Eqs. (57) and (64) with

$$\begin{aligned}\Lambda_s&=\frac{\varepsilon-\varepsilon_1}{4\pi}d,\\ \Lambda_\kappa&=\frac{\varepsilon-\varepsilon_1}{4\pi}d,\\ \Lambda_z&=\frac{\varepsilon_1}{\varepsilon}\frac{\varepsilon-\varepsilon_1}{4\pi}d.\end{aligned} \tag{97}$$

From Eqs. (65) and (70) we can then identify

$$\begin{aligned}n_{os}&=\frac{i\tilde{\omega}^2}{2w_1}(\varepsilon-\varepsilon_1)d\\ n_{o\kappa}&=\frac{iw_1}{2\varepsilon_1}(\varepsilon-\varepsilon_1)d\\ n_{oz}&=\frac{i\kappa^2}{2w_1}\frac{\varepsilon-\varepsilon_1}{\varepsilon}d.\end{aligned} \tag{98}$$

In the limit of $\varepsilon_1\to 1$ this agrees with an approximate bulk-selvedge treatment developed many years ago [17], where the validity of the approximation was also discussed.

4. SENSING EXAMPLES

As examples of how our approach will be useful in addressing structures important for sensing applications, we consider two WG sensor schemes in which a two-dimensional array of NPs is deposited on the surface of a simple WG. The WG itself consists of a cladding with relative permittivity ε_1, a guide layer with relative permittivity ε_2 and thickness D, and a substrate of relative permittivity ε_3; typically $\varepsilon_2>\varepsilon_3>\varepsilon_1$. The first scheme we consider involves using the modified WG structure to sense a change in the bulk refractive index of the cladding, and the second involves using it to detect the presence of species adsorbed onto the NPs. To analyze both of these we use the toy models introduced above to describe the layer of NPs, and so our analysis should only be considered qualitative. In later publications we will turn to more realistic calculations. Yet the results here demonstrate the potential of these types of sensors and illustrate their competitiveness with other sensing structures.

A. Waveguide Mode Change Due to Surface Nanoparticle Array

A first step in the analysis of either sensor is to consider the effect of NPs alone on the WG structure. For NPs of spherical shape arranged in a square lattice with lattice constant a, in the dipole limit the dimensionless tensor S (92) is given by

$$S=\frac{1}{\varepsilon_1}A\left(\frac{1}{2}\hat{\mathbf{x}}\hat{\mathbf{x}}+\frac{1}{2}\hat{\mathbf{y}}\hat{\mathbf{y}}-\hat{\mathbf{z}}\hat{\mathbf{z}}\right)+\frac{1}{\varepsilon_1}B(\bar{h})\left(\frac{1}{2}\hat{\mathbf{x}}\hat{\mathbf{x}}+\frac{1}{2}\hat{\mathbf{y}}\hat{\mathbf{y}}+\hat{\mathbf{z}}\hat{\mathbf{z}}\right), \tag{99}$$

with

$$A=\sum_{m,n}{}'\frac{1}{(m^2+n^2)^{3/2}}\simeq 9.03, \qquad \text{(square lattice)} \tag{100}$$

where the sums are over integers, the prime indicating that the term with $m=n=0$ is not included, and

$$\begin{aligned}B(\bar{h})&=\frac{\varepsilon_2-\varepsilon_1}{\varepsilon_2+\varepsilon_1}\sum_{m,n}\frac{3\bar{h}^2-[m^2+n^2+\bar{d}^2]}{[m^2+n^2+(\bar{h})^2]^{5/2}}\\ &=\frac{\varepsilon_2-\varepsilon_1}{\varepsilon_2+\varepsilon_1}\sum_{m,n}(2\pi)^2\sqrt{m^2+n^2}e^{-2\pi\left(\bar{h}\sqrt{m^2+n^2}\right)},\\ &\quad\text{(square lattice)}\end{aligned} \tag{101}$$

where m and n range over all integers, $\bar{h}\equiv 2h/a$, and $\bar{d}=2d/a$; in the second expression for $B(\bar{h})$ we have converted the sum to one over the reciprocal space lattice [32]; h is the height of the NP layer above the WG surface. For a disordered arrangement of NPs the corresponding expression [Eq. (94)] for S can be worked out analytically, and we find

$$\begin{aligned}A&=2\pi\sqrt{\pi}\simeq 11.14,\\ B(\bar{h})&=\frac{\varepsilon_2-\varepsilon_1}{\varepsilon_2+\varepsilon_1}\left[\frac{1}{\bar{h}^3}-\frac{2}{(2\bar{h}^2+\pi^{-1})^{3/2}}\right],\\ &\quad\text{(random arrangement)}\end{aligned} \tag{102}$$

where $\bar{h}=2h/\sqrt{\mathcal{A}}$. The values of A from Eqs. (100) and (102) are of the same order, as are the values of B from Eqs. (101) and (102) for the values of h we choose below. So there is no qualitative difference that arises from using one or the other of Eqs. (100) and (102); to be definite we use Eqs. (100) and (101) in our calculations below.

With the tensor S specified we can determine the tensor Λ from Eq. (93), and the dimensionless parameters n_{os}, $n_{o\kappa}$, n_{oz} follow from Eqs. (64), (65), and (70). For simplicity, we consider only the lowest order s-polarized WG mode and the effect on it of the NP layer; the results for the lowest order p-polarized WG mode are qualitatively the same for the range of parameters considered here. We find

$$n_{os}=\frac{\frac{(\varepsilon-\varepsilon_1)}{(\varepsilon+2\varepsilon_1)}C}{1-\frac{(\varepsilon-\varepsilon_1)}{(\varepsilon+2\varepsilon_1)}\frac{b^3}{a^3}\left(\frac{A+B(\bar{h})}{2}\right)}, \tag{103}$$

where ε is the relative permittivity of the NPs, and

$$C\equiv\frac{2\pi i\varepsilon_1\tilde{\omega}}{w_1}(\tilde{\omega}a)\frac{b^3}{a^3}.$$

The reflection coefficient [Eq. (75)] for s-polarization can then be written as

$$r=C\gamma, \tag{104}$$

where

$$\gamma \equiv \frac{\frac{(\varepsilon-\varepsilon_1)}{(\varepsilon+2\varepsilon_1)}}{1-\frac{(\varepsilon-\varepsilon_1)}{(\varepsilon+2\varepsilon_1)}C'}, \tag{105}$$

$$C' \equiv C + \frac{b^3}{a^3}\frac{A+B(\bar{h})}{2} \tag{106}$$

Near the condition for a WG mode the field in the cladding is evanescent, so $w_1 = iq$, with q a real and positive number; thus C and C' are real for a lossless WG.

With the addition of NP array, the WG mode wavenumber κ_o will change according to Eq. (83):

$$\kappa_o \to \kappa_o' = \kappa_o + r\rho_{13} = \kappa_o + \rho_{13}C\gamma, \tag{107}$$

where there are just $N = 3$ materials in the multilayer structure we consider. For a lossless WG ρ_{13}, presented in Eq. (E7) of Appendix E, will also be real. But if ε is complex, then γ will be as well, and so will $\kappa_o' - \kappa_o$. We refer to $\mathrm{Re}(\kappa_o' - \kappa_o)$ as the "mode shift," the change in wavenumber of the WG mode due to the presence of the NPs. The imaginary part of $(\kappa_o' - \kappa_o)$ describes how the amplitude of the WG mode will decay under propagation due to the presence of the NPs, and so we can introduce an absorption coefficient $\alpha_{abs} = 2\ \mathrm{Im}(\kappa_o' - \kappa_o) = 2\ \mathrm{Im}(r\rho_{13})$.

We can now investigate how these quantities depend on the WG structure and the NPs. Using Eq. (E7) for ρ_{13}, together with the assumption that the refractive indices of the WG system ε_1, ε_2 and ε_3 are not frequency dependent, we find that the product $\rho_{13}C$ scales with vacuum wavelength λ according to

$$\rho_{13}C = f(D/\lambda)/\lambda^2, \tag{108}$$

where f also depends implicitly on the three refractive indices of the WG system. For a sample calculation we consider an ion-exchanged WG with (frequency independent) $n_1 = 1.0$, $n_2 = 1.535$ and $n_3 = 1.51967$, and with an effective thickness $D = 3$ μm. This corresponds to experimentally determined parameters in [14] at a wavelength of $\lambda = 532$ nm. We assume the bare WG is itself ideal, with no loss due to scattering or absorption. For these parameters, $f(D/\lambda)$ is shown in Fig. 5. There is a minimum value of D for which a WG mode can exist; for the lowest order s-polarized mode we consider, that cutoff is given [16] by

$$\left(\frac{D}{\lambda}\right)_{\text{cut-off}} = \frac{1}{2\pi(\varepsilon_2-\varepsilon_3)^{1/2}}\tan^{-1}\left(\frac{\varepsilon_3-\varepsilon_1}{\varepsilon_2-\varepsilon_3}\right)^{1/2},$$

which has a numerical value of roughly 1 for the parameters used here. For values of D close to this cutoff, the coupling parameter $\lambda^2\rho_{13}C$ is small, because the field extends over a large region in the cladding, most of it removed from the NP layer; for values of D much larger than the cutoff, the coupling parameter is small, because the field is largely confined within the guide, away from the NP layer. We defer to later publications the application of WG design to optimize the performance of sensing structures such as those we consider here.

We now turn to the factor γ [Eq. (105)]; we take ε to be that of bare gold metal $\varepsilon = \varepsilon_m(\omega)$, for which we use the dielectric function of Johnson and Christy [33]. To treat the material dispersion of the dielectrics, at least approximately, we take the substrate index to be that for BK7 glass and keep a fixed difference between the index of the guide and the substrate of 0.01533. In Fig. 6 we show the absorption coefficient α_{abs} induced in the WG mode by the NPs. There is a maximum at λ close to 520 nm, just as there is in the extinction spectrum of a single spherical GNP. When the radius b of the NP increases, or the lattice constant a decreases, we see a redshift of the absorption peak and an increase in the amount of absorption. For example, when the particle radius is increased from

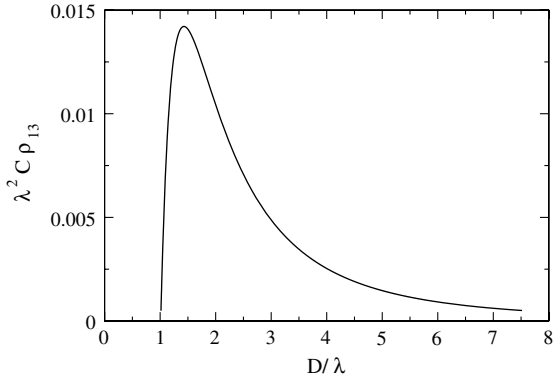

Fig. 5. $\lambda^2\rho_{13}C$ versus its argument D/λ, as discussed in the text. The refractive indices chosen are $n_1 = 1.0$, $n_2 = 1.535$, and $n_3 = 1.51967$. The graph indicates that there is a minimum value of WG thickness D below which a WG mode cannot be supported.

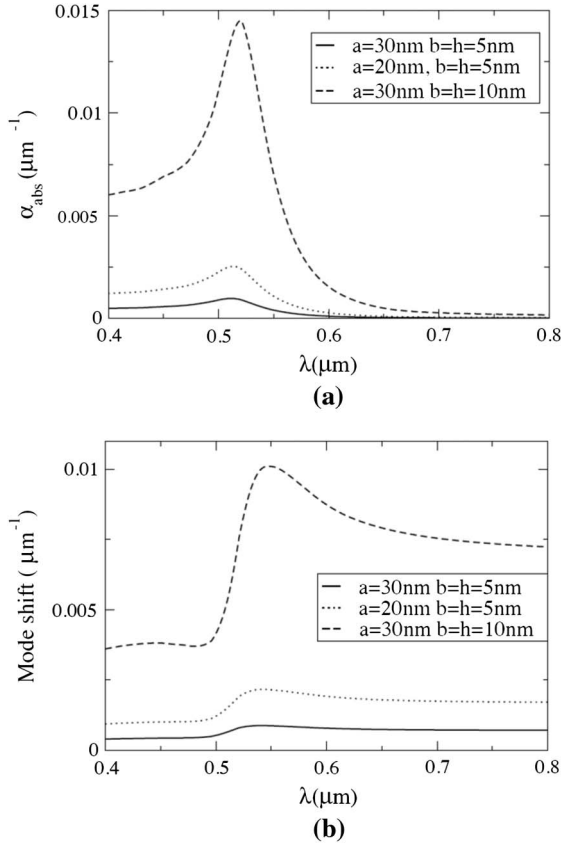

Fig. 6. (a) Absorption coefficient α_{abs} as a function of wavelength for arrays of GNPs on the surface of the WG. The thickness of the guiding layer $D = 3$ μm, and the indices are those given or the maximum response in Fig. 5. (b) The mode shift $\mathrm{Re}(\kappa_o' - \kappa_o)$ for the same structures.

$b = 5$ nm to $b = 10$ nm, the absorption coefficient increases more than eightfold, and the peak for absorption is redshifted from 511 to 520 nm. For $b = 5$ nm, but varying the lattice constant from $a = 30$ nm to $a = 20$ nm, we see a similar effect, though the magnitude for both the increase and peak shift are much smaller. We also plot the mode shift $\mathrm{Re}(\kappa_o' - \kappa_o)$.

The behavior displayed can be easily understood from the form [Eq. (105)] of γ, which is mainly responsible for the frequency dependence of both the absorption coefficient and the mode shift. Taking $\varepsilon_m^r(\omega) = \mathrm{Re}(\varepsilon_m(\omega))$ and $\varepsilon_m^i(\omega) = \mathrm{Im}(\varepsilon_m(\omega))$, we have

$$\mathrm{Im}\,\gamma = \frac{3\varepsilon_m^i(\omega)\varepsilon_1}{(\varepsilon_m^i(\omega))^2(1-C')^2 + (\varepsilon_m^r(\omega)(1-C') + \varepsilon_1(C'+2))^2}, \tag{109}$$

where to a first approximation we can evaluate C' at κ_o and the frequency ω of interest. In the optical range $\varepsilon_m^i(\omega)$ is approximately constant, and so this equation can be thought of as approximately a Lorentz-like function with a maximum at $\varepsilon_m^r(\omega)(1-C') + (C'+2)\varepsilon_1 = 0$ and a width $\varepsilon_m^i(\omega)(1-C')$. The peak wavelength is thus given by the condition

$$\varepsilon_m^r(\omega) = (C'+2)/(C'-1)\varepsilon_1. \tag{110}$$

We have numerically found good agreement between the peak wavelength from Eqs. (109) and (110).

B. Bulk Index Nanoparticle-Waveguide Sensor

We now turn to the effect of a change in the cladding index on the properties of the NP-covered WG. In particular, the change in the peak of the absorption of the WG mode will provide an indication of the change in the bulk refractive index $n_1 = \sqrt{\varepsilon_1}$. Used in this way, we refer to our NP-covered WG structure as a "bulk index nanoparticle-waveguide sensor" (BNWS). A sensor with which this can be compared is a "colloidal nanoparticle sensor" (CNS), where the change in the extinction spectrum of a dilute concentration of NPs is an indication of the change in the host refractive index. For small NPs the extinction spectrum is almost indistinguishable from the absorption spectrum, and so in the dilute limit we can characterize a CNS by studying the absorption cross section σ_{abs} of a single NP. In the dipole approximation, that is given by

$$\sigma_{\mathrm{abs}}/(\pi b^2) = 4\tilde{\omega}\sqrt{\varepsilon_1}\, b\, \mathrm{Im}\left[\frac{\varepsilon - \varepsilon_1}{\varepsilon + 2\varepsilon_1}\right] \tag{111}$$

(see, e.g., van de Hulst [34]). Again taking the relative permittivity of the NP to be that of bulk gold metal, the peak position is associated with $\varepsilon_m^r(\omega) \approx -2\varepsilon_1$, as is well known; this corresponds to the $C' = 0$ limit of Eq. (110), as would be expected, since $C' = 0$ corresponds to the limit when the NPs on the WG surface are far from each other, and the single particle response is dominant.

Since in the optical range $\varepsilon_m^r(\omega)$ is to good approximation a linearly decreasing function of wavelength, for a dilute CNS the wavelength of the extinction peak changes linearly with the dielectric constant of the host medium. In a BNWS, a nonvanishing C' in Eqs. (109) and (110) will lead to a larger slope in the dependence of $\varepsilon_m^r(\omega) - \varepsilon_1$ on λ, and so for the same change in ε_1 there is a larger change in the peak wavelength than in a CNS. This is shown in Fig. 7 for a NP structure with $a = 30$ nm, $b = h = 10$ nm. We also note that the shapes of the loss spectrum in the two sensors are different. For $C' > 0$ the peak is better defined, as we see from the calculations in Fig. 8, where we compare σ_{abs} from Eq. (111) with $\mathrm{Im}\gamma$ from Eq. (109), both normalized to a maximum value of unity. This should make the resolution of the loss peak easier for a BNWS than for a CNS.

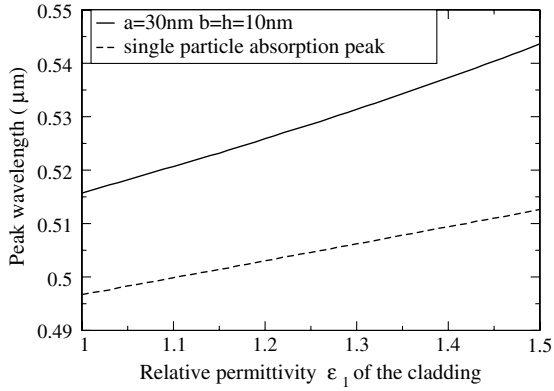

Fig. 7. Peak wavelengths of the absorption curve as a function of cladding relative permittivity. The dotted curve represents a single particle, and the solid curve shows the NP-coated WG. The WG properties are as specified in Fig. 6, and the NP array parameters are given in the legend.

We can also compare our BNWS with the use of a surface plasmon to monitor the index of the cladding; we refer to this latter scheme as a "bulk index surface plasmon sensor" (BSPS). Putting aside the details of how the bound modes can be excited and detected in either the BNWS or the BSPS, we just compare a sensitivity parameter similar to that used earlier [35]:

$$H \equiv \frac{(\partial \mathrm{Re}[\kappa_o'])/(\partial\varepsilon_1)}{\mathrm{Im}[\kappa_o']}, \tag{112}$$

which gives a ratio of the shift of the peak of the loss with change in cladding index to the width of the loss peak, and is itself a function of the original cladding relative permittivity.

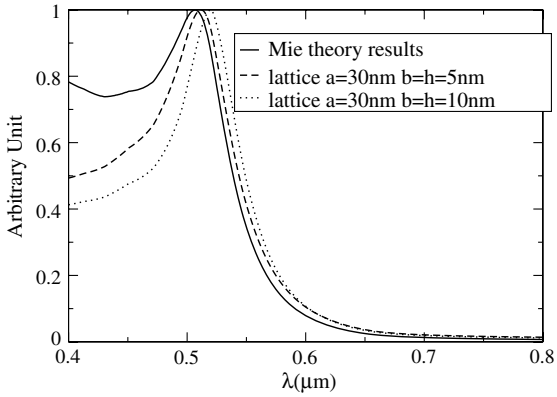

Fig. 8. Mie theory calculations of the absorption cross section of a single GNP compared with the absorption spectrum of a WG, with parameters given in Fig. 6, when coated with an array of GNPs. The spherical particles are just resting on top of the WG. All curves have been normalized to have a maximum of unity.

For a BNWS, κ_o' is the WG mode resonance in the presence of the NPs [Eq. (107)], while for the BSPS it is the (complex) wavenumber $\kappa_{\rm SP}$ of the surface plasmon,

$$\kappa_{\rm SP} = \tilde{\omega}\sqrt{\frac{\varepsilon_m(\omega)\varepsilon_1}{\varepsilon_m(\omega)+\varepsilon_1}}, \tag{113}$$

where we assume bulk gold metal as the substrate. The sensitivity parameters [Eq. (112)] are compared in Fig. 9 for a NP structure with the same parameters as used previously, $a = 30$ nm, $b = h = 10$ nm. We see that the BNWS is generally competitive with the BSPS, and in fact surpasses it for relative cladding permittivities larger than about 1.4.

C. Coated Nanoparticle-Waveguide Sensor

We now consider using an NP-covered WG to detect the presence of molecules that adsorb onto the NPs, providing a coating. The shift in the peak of the loss spectrum of the WG mode here provides an indication of the adsorbed molecules. Used in this way, we refer to our NP-covered WG structure as a "coated nanoparticle-waveguide sensor" (CNWS). Scenarios where instead the dielectric constant of the NPs is changed by absorption rather than adsorption could be treated in a similar way. Treating both the original NPs and their coated successors in the dipole approximation, the coated NPs can be modeled as uniform spheres of the same size but with an effective relative permittivity given by

$$\varepsilon_{\rm av} = \varepsilon_{\rm coat}\frac{1+2\frac{b_{\rm core}^3}{b_{\rm coat}^3}\frac{\varepsilon-\varepsilon_{\rm coat}}{\varepsilon+2\varepsilon_{\rm coat}}}{1-\frac{b_{\rm core}^3}{b_{\rm coat}^3}\frac{\varepsilon-\varepsilon_{\rm coat}}{\varepsilon+2\varepsilon_{\rm coat}}}, \tag{114}$$

where ε and $\varepsilon_{\rm coat}$ are, respectively, the relative permittivities of the core and coating, and $b_{\rm core}$ and $b_{\rm coat}$ are, respectively, the radii of the original core and the coated NP. We take the core to be gold metal, with $\varepsilon = \varepsilon_m(\omega)$, and consider a cladding with $\varepsilon_1 = 1$. The wavenumber κ_o' of the modified WG mode is then given by Eqs. (105)–(107), but with ε replaced by $\varepsilon_{\rm av}$ and b replaced by $b_{\rm coat}$.

As a simple model calculation, we consider NPs with a lattice constant $a = 30$ nm of radius $b_{\rm core} = 5$ nm, with a dielectric coating of fixed thickness 5 nm as well ($b_{\rm coat} = 10$ nm, $h = 10$ nm; see Fig. 10); we imagine that the relative coating permittivity $\varepsilon_{\rm coat}$ changes due to adsorption. We show in Fig. 11(a) the mode shift as $\varepsilon_{\rm coat}$ varies from 1.0 to 1.5. The shift increases roughly linearly over the entire frequency range we consider and is largest at about $\lambda = 550$ nm. However, as shown in Fig. 11(b), the absorption is large there, and so detecting the mode shift would not be particularly easy. To characterize the sensitivity of the structure in a simple way, we can introduce a sensitivity parameter G similar to that of Eq. (112),

$$G = \frac{(\partial {\rm Re}\kappa_o')/(\partial\varepsilon_{\rm coat})}{{\rm Im}\,\kappa_o'} = \frac{(\partial {\rm Re}\,\gamma)/(\partial\varepsilon_{\rm coat})}{{\rm Im}\,\gamma} \tag{115}$$

itself a function of the $\varepsilon_{\rm coat}$ about which the change is presumed to occur. We show this parameter in Fig. 12, where it is clear that, at least by this measure, detection will be most effective at larger wavelengths within the range we consider.

For reference we can compare this with a sensor relying on the shift of a surface plasmon excitation due to the change in the permittivity of an overlayer. To a first approximation in determining the mode shift of the surface plasmon, we can consider a semi-infinite gold medium as the substrate. In the absence of an overlayer, the SPR [Eq. (113)] is signaled by the pole of the Fresnel reflection coefficient, as detailed in Appendix E. To make a comparison corresponding to the same amount of coating as assumed in our CNWS, we add

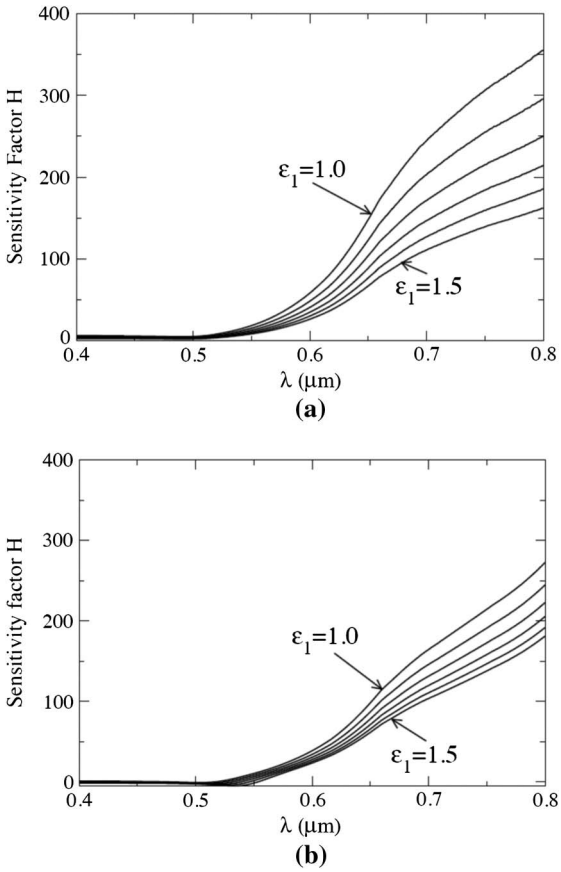

Fig. 9. Sensitivity factor H for (a) a BSPS and (b) a BNWS, as described in the text. In the latter example we take $a = 30$ nm, $b = h = 10$ nm. The cladding's relative permittivity ε_1 ranges from 1.0 (top curve) to 1.5 (bottom curve) in increments of 0.1.

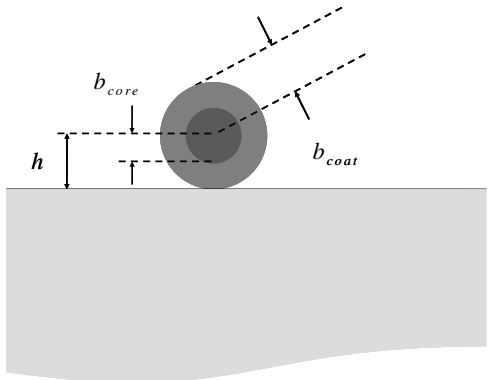

Fig. 10. Coated NP parameters. The radius of the GNP core is $b_{\rm core}$, and that of the coated NP is $b_{\rm coat}$. The height of the GNP center from the WG h is chosen to be the same as $b_{\rm coat}$.

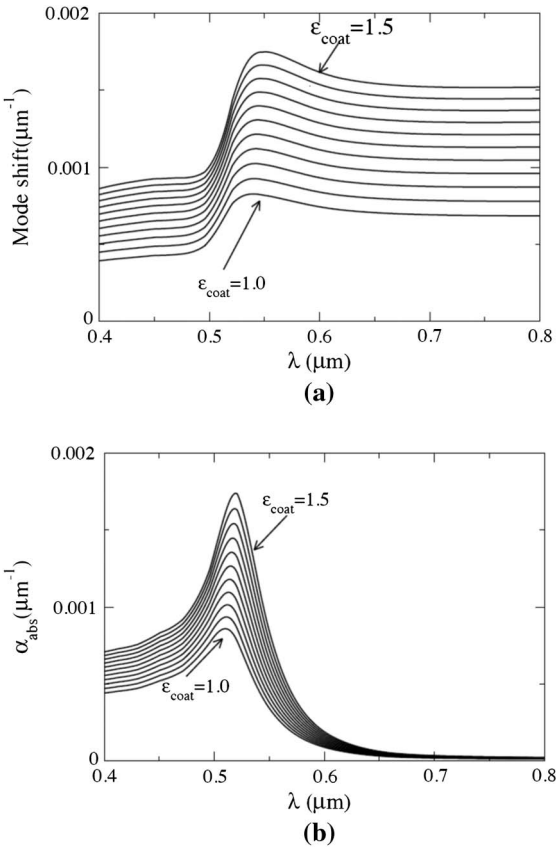

Fig. 11. Modification of mode properties of an NP-coated WG, as the relative permittivity $\varepsilon_{\text{coat}}$ of the coating is varied from $\varepsilon_{\text{coat}} = 1.0$ (bottom curve) to $\varepsilon_{\text{coat}} = 1.5$ (top curve) in increments of 0.05. (a) The mode shift $\text{Re}(\kappa_o' - \kappa_o)$, (b) the absorption coefficient α_{abs}. The mode shift is high at the same wavelength as the absorption.

a thin layer of analyte with thickness $4\pi(b_{\text{coat}}^3 - b_{\text{core}}^3)/(3a^2)$, which here is about 4 nm. To get a simple but accurate estimate of the change of the surface plasmon wavenumber [Eq. (113)] due to the overlayer, we can use the analog of Eq. (107),

$$\kappa_{\text{SP}} \to \kappa_{\text{SP}}' = \kappa_{\text{SP}} + r_p \rho_{1m}, \tag{116}$$

[see Eq. (83) and the derivation leading to it] where ρ_{1m} is given by Eq. (E3) of Appendix E, and r_p is given by Eq. (77),

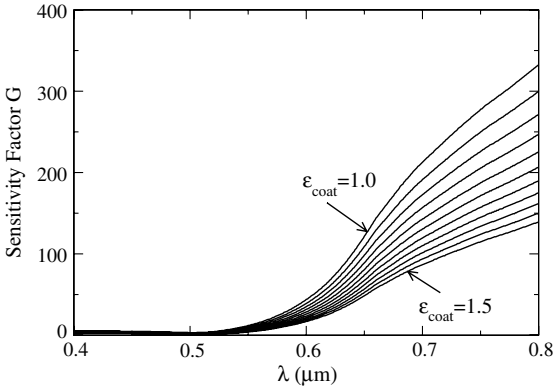

Fig. 12. Sensitivity factor G for WG sensing. The relativity permittivity of the analyte $\varepsilon_{\text{coat}}$ varies from $\varepsilon_{\text{coat}} = 1.0$ (top curve) to $\varepsilon_{\text{coat}} = 1.5$ (bottom curve) in increments of 0.05.

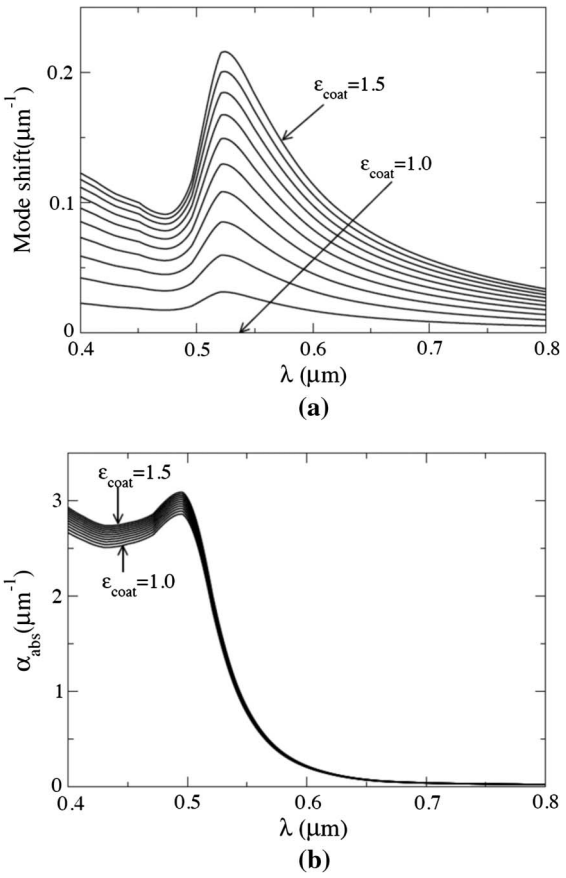

Fig. 13. Same plots as in Fig. 11, but for the surface plasmon sensor.

where n_{oz} and $n_{o\kappa}$ in Eq. (71) are given by Eq. (98), with ε replaced by $\varepsilon_{\text{coat}}$. In Fig. 13 we plot the mode shift $\text{Re}(\kappa_{\text{SP}}' - \kappa_{\text{SP}})$ and the absorption coefficient $\alpha_{\text{abs}} = 2\,\text{Im}(\kappa_{\text{SP}}')$ as a function of wavelength for different values of $\varepsilon_{\text{coat}}$. The corresponding sensitivity parameter G, given by the first term of Eq. (115) with κ_o' replaced by κ_{SP}', is plotted in Fig. 14. Comparing with Figs. 11 and 12, we see that the surface plasmon structure has a larger mode shift but also much stronger absorption; the sensitivity parameter is thus much smaller than for the CNWS. Keeping h and b_{core} fixed and varying $b_{\text{coat}} - b_{\text{core}}$ from 1 to 5 nm, we find that the CNWS still has a higher sensitivity G than the surface plasmon sensor,

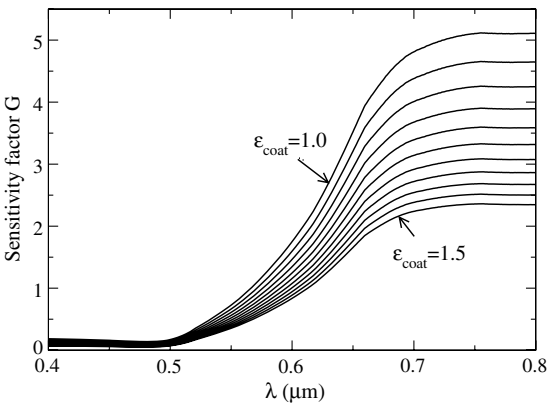

Fig. 14. Same plot as in Fig. 12, but for the surface plasmon sensor.

indicating that its better performance is robust over a wide range of sensing regimes.

5. CONCLUSIONS

We have presented an approach for calculating optical propeties of a selvedge layer on top of a multilayer structure, where the selvedge layer is taken to have a height much less than the wavelength of light, and with optical susceptibility variations in the plane on distance scales much less than the wavelength of light. By treating the electrostatic component of the field in general numerically, and the radiative component analytically, the calculation of the response of the selvedge can be simplified and transfer matrices for it constructed. In sensing applications the selvedge will typically consist of metallic NPs, coated by adsorbed sensing targets or used to help detect a change in the bulk refractive index of the cladding. Within a simple model of treating spherical metallic NPs in the point dipole limit, we have shown that a WG sensor based on this design is promising for both these sensing applications. In future communications we plan to turn to more realistic analyses of metallic NP arrays. This can be done by including the effects of higher order multipole moments of the NPs, or by direct numerical calculation of Eqs. (58) and (59).

We close with a discussion of some straightforward generalizations of our results.

First, we note that although we have treated the index n_1 of the cladding as real, the general equations can be easily extended to treat a complex n_1 if the imaginary part is not too large, as would be expected for realistic claddings. Second, we note that for some systems and some frequencies there will be "isolated selvedge" resonances, where the Fresnel coefficients r and t appearing in Eq. (80) diverge. Here the multilayer can be thought of as modifying the selvedge resonance, rather than the selvedge modifying the multilayer (in our case WG) resonance, as we studied in this paper. We will return to these problems in a later communication.

Third, we note that while we have focused on the poles of Fresnel coefficients, the formalism we have developed allows for a study of the full optical response of the selvedge-coated multilayer, and thus should be useful for the study of other optical sensing strategies, such as Raman scattering. Finally, we note that the derivation of the selvedge response of the planar layer given in Section 3.C can be easily extended to the case where the region $0 < z < d$ is characterized by a relative dielectric tensor of the form

$$\varepsilon = \hat{\mathbf{z}}\,\hat{\mathbf{z}}\,\varepsilon_\perp + (\hat{\mathbf{x}}\,\hat{\mathbf{x}} + \hat{\mathbf{y}}\,\hat{\mathbf{y}})\varepsilon_\parallel. \tag{117}$$

Instead of Eq. (97), we find

$$\begin{aligned}\Lambda_s &= \frac{\varepsilon_\parallel - \varepsilon_1}{4\pi} d,\\ \Lambda_\kappa &= \frac{\varepsilon_\parallel - \varepsilon_1}{4\pi} d,\\ \Lambda_z &= \frac{\varepsilon_1}{\varepsilon_\perp}\frac{\varepsilon_\perp - \varepsilon_1}{4\pi} d.\end{aligned} \tag{118}$$

Now suppose that in considering a *general* selvedge region, we find a response of the form of Eq. (63) with a tensor Λ of the form of Eq. (64) with $\Lambda_s = \Lambda_\kappa \equiv \Lambda_\parallel$. Then we can *define* effective quantities $\varepsilon_\parallel^{\text{eff}}$ and $\varepsilon_\perp^{\text{eff}}$ so that Eq. (118) is satisfied. That is, we put

$$\begin{aligned}\frac{\varepsilon_\parallel^{\text{eff}}}{\varepsilon_1} &= 1 + \frac{4\pi\Lambda_\parallel}{d\varepsilon_1},\\ \frac{\varepsilon_\perp^{\text{eff}}}{\varepsilon_1} &= \left(1 - \frac{4\pi\Lambda_z}{d\varepsilon_1}\right)^{-1},\end{aligned}$$

where we must choose a nominal d. Once this is done, within our approximations our selvedge region is optically equivalent to uniform thin film of thickness d, and a dielectric tensor of the form of Eq. (117) is placed on top of our original multilayer structure. Of course, this formal equivalence should not lead to the misunderstanding that $\varepsilon_\parallel^{\text{eff}}$ and $\varepsilon_\perp^{\text{eff}}$ depend only on the optical properties of the material in the selvedge; recall that Λ depends on the effect of the image fields as well, and they depend on the optical properties of the material right below the selvedge. Nonetheless, once this *effective thin film model* for the selvedge is identified, it can be used, at least in a first approximation, to treat a selvedge on a channel WG structure, where Λ is determined from the corresponding planar structure. The modes of such channel WGs must be determined numerically, but with an effective thin-film model for the selvedge, and thus for its modification by sensing targets, we can leverage our treatment here to consider the kind of channel structures that will be useful in multiplexed sensing devices.

APPENDIX A: THE GREEN FUNCTION $G^o(\mathbf{r})$

The Green function $G^o(\mathbf{r})$ yields the electric field amplitude at $\mathbf{r}$ produced by a point dipole oscillating at frequency ω at the origin in a uniform medium of relative permittivity $\varepsilon_1 = n_1^2$, and is given by

$$\begin{aligned}4\pi\epsilon_0 G^o(\mathbf{r}) = {}& \frac{3\hat{\mathbf{r}}\,\hat{\mathbf{r}} - U}{\varepsilon_1}\left(\frac{e^{i\tilde{\omega}n_1 r}}{r^3} - \frac{i\tilde{\omega}n_1 e^{i\tilde{\omega}n_1 r}}{r^2}\right)\\ &+ \frac{\tilde{\omega}^2(U - \hat{\mathbf{r}}\,\hat{\mathbf{r}})e^{i\tilde{\omega}n_1 r}}{r} - \frac{4\pi}{3\varepsilon_1}\delta(\mathbf{r})U,\end{aligned} \tag{A1}$$

where $U \equiv \hat{\mathbf{x}}\,\hat{\mathbf{x}} + \hat{\mathbf{y}}\,\hat{\mathbf{y}} + \hat{\mathbf{z}}\,\hat{\mathbf{z}}$ is the unit dyadic, $\tilde{\omega} = \omega/c$, $\mathbf{r} = \mathbf{R} + \hat{\mathbf{z}}z$, with $\mathbf{R} = (x, y)$, and $\hat{\mathbf{r}} \equiv \mathbf{r}/r$, where $r \equiv |\mathbf{r}|$, with the convention that integrals over $\mathbf{r}$ are to be first done over $\hat{\mathbf{r}}$ and then over r; this makes integrals that all appear well-defined (see Sections 9.1 and 9.2 of [30]). We split $G^o(\mathbf{r})$ into a component $G_L^o(\mathbf{r})$ that identifies the longitudinal component of the electric field (that part with vanishing curl) and a component $G_T^o(\mathbf{r})$ that identifies the transverse component of the electric field (that part with vanishing divergence); $G_L^o(\mathbf{r})$ is easily recovered as the $c \to \infty$ limit of $G^o(\mathbf{r})$,

$$4\pi\epsilon_0 G_L^o(\mathbf{r}) = \frac{3\hat{\mathbf{r}}\,\hat{\mathbf{r}} - U}{\varepsilon_1 r^3} - \frac{4\pi}{3\varepsilon_1}\delta(\mathbf{r})U, \tag{A2}$$

and the transverse component $G_T^o(\mathbf{r}) = G^o(\mathbf{r}) - G_L^o(\mathbf{r})$. For $\tilde{\omega}n_1 r \ll 1$ we find Eq. (32).

APPENDIX B: THE GREEN FUNCTION $G^R(\mathbf{R} - \mathbf{R}'; z, z')$

To derive an expression for $G^R(\mathbf{R} - \mathbf{R}'; z, z')$, we being with the Fourier components [Eq. (23)] of $G^o(\mathbf{R} - \mathbf{R}'; z, z')$,

$$G^o(\kappa;z,z') = \frac{i\tilde{\omega}^2}{2\epsilon_0 w_1}(\hat{\mathbf{s}}\,\hat{\mathbf{s}} + \hat{\mathbf{p}}_{1+}\hat{\mathbf{p}}_{1+})\theta(z-z')e^{iw_1(z-z')} + \frac{i\tilde{\omega}^2}{2\epsilon_0 w_1}(\hat{\mathbf{s}}\,\hat{\mathbf{s}} + \hat{\mathbf{p}}_{1-}\hat{\mathbf{p}}_{1-})\theta(z'-z)e^{iw_1(z'-z)} - \frac{\hat{\mathbf{z}}\,\hat{\mathbf{z}}}{\epsilon_0\varepsilon_1}\delta(z-z') \tag{B1}$$

(see, e.g., [31]) with $\theta(z) = 1, 0$ as $z > 0, < 0$, with w_m defined according to Eq. (37), and the unit vectors $\hat{\mathbf{s}}$ and $\hat{\mathbf{p}}_{m\pm}$ defined according to Eqs. (38) and (39). We can now immediately determine $G^R(\kappa;z,z')$, since the downward wave in the second term of the right-hand side of Eq. (B1) will be reflected from the multilayer structure, and in the course of this the polarization direction of the p-polarized wave will be changed. Keeping track of the phases due to the $e^{\pm iw_1 z}$ terms we then have simply [36]

$$G^R(\kappa;z,z') = \frac{i\tilde{\omega}^2}{2\epsilon_0 w_1}(\hat{\mathbf{s}}R^s_{1N}\hat{\mathbf{s}} + \hat{\mathbf{p}}_{1+}R^p_{1N}\hat{\mathbf{p}}_{1-})e^{iw_1(z+z')}, \tag{B2}$$

which we use for $z > 0$ and $z' > 0$. The Fresnel reflection coefficients R^s_{1N} and R^p_{1N}, both functions of κ, are mentioned after Eq. (39); they give the amplitude of a reflected plane wave to the amplitude of a plane wave incident on the bare multilayer structure from $z > 0$, and can be written in terms of propagation factors and the fundamental Fresnel coefficients at an interface [31]. Those fundamental reflection (transmission) coefficients r_{ij} (t_{ij}), for a beam incident from medium i on medium j, are given by

$$r^s_{ij} = \frac{w_i - w_j}{w_i + w_j}, \qquad t^s_{ij} = \frac{2w_i}{w_i + w_j} \tag{B3}$$

for s-polarized light, where the w_i are defined by Eq. (37), and by

$$r^p_{ij} = \frac{w_i\varepsilon_j - w_j\varepsilon_i}{w_i\varepsilon_j + w_j\varepsilon_i}, \qquad t^p_{ij} = \frac{2n_i n_j w_i}{w_i\varepsilon_j + w_j\varepsilon_i} \tag{B4}$$

for p-polarized light. We can write

$$R_{1N} = r_{12} + \frac{t_{12}R_{2N}t_{21}e^{2iw_2D_2}}{1 - R_{2N}r_{21}e^{2iw_2D_2}} \tag{B5}$$

for both s- and p-polarized coefficients, where R_{2N} is the reflection coefficient from the bottom of layer 2 across the rest of the multilayer structure; relations such as this can easily be worked out using transfer matrices [31]. A similar expression can then be worked out for R_{2N} in terms of R_{3N} and fundamental Fresnel coefficients [Eq. (B3) or (B4)] as appropriate, and so ultimately an expression for R_{1N} results. A formal expression for $G^R(\mathbf{R}-\mathbf{R}';z,z')$ then follows from Fourier superposition [Eq. (23)].

APPENDIX C: GREEN FUNCTION LIMITS AND THE IMAGE POLARIZATION

We begin by working out $G^R_{I,C}(\kappa;z,z')$ as defined by Eq. (42) and the following text. Taking the first of the double limits $\kappa c/\omega \to \infty$ and $\kappa D_2 \to \infty$, we find

$$w_l \to i\kappa$$

for all l, and so from Eqs. (B3) and (B4) we have

$$r^s_{ij} \to 0, \qquad r^p_{ij} \to \frac{\varepsilon_j - \varepsilon_i}{\varepsilon_j + \varepsilon_i}.$$

Also, $e^{2iw_2D_2} \to e^{-2\kappa D_2}$, and taking the second of the limits $e^{2iw_2D_2} \to 0$; so from Eq. (B5) we have

$$R^s_{1N} \to 0, \qquad R^p_{1N} \to \frac{\varepsilon_2 - \varepsilon_1}{\varepsilon_2 + \varepsilon_1}.$$

Then, working out the remaining terms in $G^R(\kappa;z,z')$ [Eq. (B2)] in the limit $\kappa c/\omega \to \infty$, we find

$$G^R_I(\kappa;z,z') = \frac{\kappa}{2\epsilon_0\varepsilon_1}\frac{\varepsilon_2 - \varepsilon_1}{\varepsilon_2 + \varepsilon_1}(\hat{\mathbf{z}}\,\hat{\mathbf{z}} + \hat{\kappa}\,\hat{\kappa} + i\hat{\mathbf{z}}\,\hat{\kappa} - i\hat{\kappa}\,\hat{\mathbf{z}})e^{-\kappa(z+z')}, \tag{C1}$$

and we therefore have

$$G^R_C(\kappa;z,z') = \frac{i\tilde{\omega}^2}{2\epsilon_0 w_1}(\hat{\mathbf{s}}R^s_{1N}\hat{\mathbf{s}} + \hat{\mathbf{p}}_{1+}R^p_{1N}\hat{\mathbf{p}}_{1-})e^{iw_1(z+z')} - \frac{\kappa}{2\epsilon_0\varepsilon_1}\frac{\varepsilon_2 - \varepsilon_1}{\varepsilon_2 + \varepsilon_1}(\hat{\mathbf{z}}\,\hat{\mathbf{z}} + \hat{\kappa}\,\hat{\kappa} + i\hat{\mathbf{z}}\,\hat{\kappa} - i\hat{\kappa}\,\hat{\mathbf{z}})e^{-\kappa(z+z')}, \tag{C2}$$

by definition negligible for $\kappa D_2 \gg 1$ and $\kappa c/\omega \gg 1$.

To make explicit the physics of $G^R_I(\kappa;z,z')$, we need first to extract the component $G^o_L(\kappa;z,z')$ of $G^o(\kappa;z,z')$, which can be identified by forming the dimensionless quantity $\kappa^{-1}G^o(\kappa;z,z')$ and taking the limit $\kappa c/\omega \to \infty$. We find

$$G^o_L(\kappa;z,z') = \frac{\kappa}{2\epsilon_0\varepsilon_1}(\hat{\mathbf{z}}\,\hat{\mathbf{z}} - \hat{\kappa}\,\hat{\kappa} - i\hat{\mathbf{z}}\,\hat{\kappa} - \hat{i}\,\hat{\kappa}\,\hat{\mathbf{z}})\theta(z-z')e^{-\kappa(z-z')} + \frac{\kappa}{2\epsilon_0\varepsilon_1}(\hat{\mathbf{z}}\,\hat{\mathbf{z}} - \hat{\kappa}\,\hat{\kappa} + i\hat{\mathbf{z}}\,\hat{\kappa} + \hat{i}\,\hat{\kappa}\,\hat{\mathbf{z}})\theta(z'-z)e^{-\kappa(z'-z)} - \frac{\hat{\mathbf{z}}\,\hat{\mathbf{z}}}{\epsilon_0\varepsilon_1}\delta(z-z'). \tag{C3}$$

For any vector field $\mathbf{V}(\mathbf{R};z)$ that is nonzero only for $z > 0$, if we define a corresponding image field $\mathbf{V}^I(\mathbf{R};z)$ according to

$$\mathbf{V}^I(\mathbf{R};z) \equiv \frac{\varepsilon_2 - \varepsilon_1}{\varepsilon_2 + \varepsilon_1}(\hat{\mathbf{z}}\,\hat{\mathbf{z}} - \hat{\mathbf{x}}\,\hat{\mathbf{x}} - \hat{\mathbf{y}}\,\hat{\mathbf{y}})\cdot\mathbf{V}(\mathbf{R};-z), \tag{C4}$$

which will vanish only for $z < 0$, or equivalently,

$$\mathbf{V}^I(\kappa;z) \equiv \frac{\varepsilon_2 - \varepsilon_1}{\varepsilon_2 + \varepsilon_1}(\hat{\mathbf{z}}\,\hat{\mathbf{z}} - \hat{\mathbf{x}}\,\hat{\mathbf{x}} - \hat{\mathbf{y}}\,\hat{\mathbf{y}})\cdot\mathbf{V}(\kappa;-z),$$

using Eqs. (C1) and (C3) we find immediately that

$$\int G_I^R(\kappa;z,z')\cdot\mathbf{V}(\kappa,z')\mathrm{d}z' = \int G_L^o(\kappa;z,z')\cdot\mathbf{V}^I(\kappa,z')\mathrm{d}z' \quad \text{(C5)}$$

for $z>0$, where we have used the fact that $\hat{\mathbf{x}}\hat{\mathbf{x}}+\hat{\mathbf{y}}\hat{\mathbf{y}}=\hat{\mathbf{s}}\hat{\mathbf{s}}+\hat{\kappa}\hat{\kappa}$. Returning to real space, from Eq. (C5) we have

$$\int G_I^R(\mathbf{R}-\mathbf{R}';z,z')\cdot\mathbf{V}(\mathbf{R}',z')dz'\mathrm{d}\mathbf{R}' = \int G_L^o(\mathbf{R}-\mathbf{R}';z,z')\cdot\mathbf{V}^I(\mathbf{R}',z')dz'\mathrm{d}\mathbf{R}'.$$

Defining $\mathbf{v}(\mathbf{R};z)$ and $\mathbf{v}^I(\mathbf{R};z)$ according to

$$\mathbf{V}(\mathbf{R};z)=e^{i\boldsymbol{\kappa}^i\cdot\mathbf{R}}\mathbf{v}(\mathbf{R};z),$$
$$\mathbf{V}^I(\mathbf{R};z)=e^{i\boldsymbol{\kappa}^i\cdot\mathbf{R}}\mathbf{v}^I(\mathbf{R};z),$$

we see that $\mathbf{v}(\mathbf{R};z)$ and $\mathbf{v}^I(\mathbf{R};z)$ satisfy the same condition [Eq. (C4)] that $\mathbf{V}(\mathbf{R};z)$ and $\mathbf{V}^I(\mathbf{R};z)$ satisfy, and also that

$$\int e^{-i\boldsymbol{\kappa}^i\cdot(\mathbf{R}-\mathbf{R}')}G_I^R(\mathbf{R}-\mathbf{R}';z,z')\cdot\mathbf{v}(\mathbf{R}',z')dz'\mathrm{d}\mathbf{R}' = \int e^{-i\boldsymbol{\kappa}^i\cdot(\mathbf{R}-\mathbf{R}')}G_L^o(\mathbf{R}-\mathbf{R}';z,z')\cdot\mathbf{v}^I(\mathbf{R}',z')dz'\mathrm{d}\mathbf{R}'. \quad \text{(C6)}$$

In the text, $\tilde{\mathbf{p}}(\mathbf{R};z)$ is the vector field $\mathbf{v}(\mathbf{R};z)$ of interest.

Finally, in this appendix we identify $G_T^o(\kappa;z,z')\equiv G^o(\kappa;z,z')-G_L^o(\kappa;z,z')$ in the limit that w_1z, w_1z', κz, and $\kappa z'$ are in magnitude all much less than unity. From Eqs. (B1) and (C3), simple algebra leads to the result

$$G_T^o(\kappa;z,z')\to\frac{1}{2\epsilon_0}\left[\frac{i\tilde{\omega}^2}{w_1}\hat{\mathbf{s}}\hat{\mathbf{s}}+\frac{1}{\varepsilon_1}\left(\frac{i\kappa^2}{w_1}-\kappa\right)\hat{\mathbf{z}}\hat{\mathbf{z}}+\frac{1}{\varepsilon_1}(iw_1+\kappa)\hat{\kappa}\hat{\kappa}\right] \equiv G_T^o(\kappa) \quad \text{for } w_1z,w_1z',\kappa z,\kappa z'\ll 1, \quad \text{(C7)}$$

independent of z and z'.

APPENDIX D: JUMP EQUATIONS

In this appendix we derive the equations relating the coarse-grained fields $\bar{\mathbf{E}}(\mathbf{R},d^+)$ and $\bar{\mathbf{E}}(\mathbf{R},0^l)$. Beginning with Eq. (24) for $\bar{\mathbf{E}}(\mathbf{R},z)$, the decomposition [Eq. (3)] for the full Green function G, and Eqs. (B1) and (B2) for the Fourier transforms of its components, we have

$$e^{-i\boldsymbol{\kappa}^i\cdot\mathbf{R}}\bar{\mathbf{E}}(\mathbf{R};d^+)=\mathcal{F}_{h+}e^{iw_1^id^+}+\mathcal{F}_{h-}e^{-iw_1^id^+} +\frac{i\tilde{\omega}^2}{2\epsilon_0w_1^i}(\hat{\mathbf{s}}^i\hat{\mathbf{s}}^i+\hat{\mathbf{p}}_{1-}^i\hat{\mathbf{p}}_{1+}^i)e^{iw_1^id^+}\cdot\int e^{-iw_1^iz'}\mathcal{P}(z')\mathrm{d}z' +\frac{i\tilde{\omega}^2}{2\epsilon_0w_1^i}(\hat{\mathbf{s}}^iR_{1N}^s(\kappa^i)\hat{\mathbf{s}}^i+\hat{\mathbf{p}}_{1+}^iR_{1N}^p(\kappa^i)\hat{\mathbf{p}}_{1-}^i)e^{iw_1^id^+} \cdot\int e^{iw_1^iz'}\mathcal{P}(z')\mathrm{d}z',$$

where as usual the superscripts i indicate that the quantities are to be evaluated at κ^i, and we have used the form of $\mathcal{F}_h(z)$ as identified in Eq. (48). Similarly,

$$e^{-i\boldsymbol{\kappa}^i\cdot\mathbf{R}}\bar{\mathbf{E}}(\mathbf{R};0^l)=\mathcal{F}_{h+}e^{iw_1^i0^l}+\mathcal{F}_{h-}e^{-iw_1^i0^l} +\frac{i\tilde{\omega}^2}{2\epsilon_0w_1^i}(\hat{\mathbf{s}}^i\hat{\mathbf{s}}^i+\hat{\mathbf{p}}_{1-}^i\hat{\mathbf{p}}_{1-}^i)e^{-iw_1^i0^l}\cdot\int e^{iw_1^iz'}\mathcal{P}(z')\mathrm{d}z' +\frac{i\tilde{\omega}^2}{2\epsilon_0w_1^i}(\hat{\mathbf{s}}^iR_{1N}^s(\kappa^i)\hat{\mathbf{s}}^i+\hat{\mathbf{p}}_{1+}^iR_{1N}^p(\kappa^i)\hat{\mathbf{p}}_{1-}^i)e^{iw_1^i0^l} \cdot\int e^{iw_1^iz'}\mathcal{P}(z')\mathrm{d}z'.$$

Each of these terms contains contributions to upward- and downward-going waves. We can write Eq. (60) (recall that there we have put $\kappa^i\to\kappa$), and identify

$$\bar{\mathbf{E}}^+(d^+)=\mathcal{F}'_{h+}(\kappa^i)e^{iw_1^id^+} +\frac{i\tilde{\omega}^2}{2\epsilon_0w_1^i}(\hat{\mathbf{s}}^i\hat{\mathbf{s}}^i+\hat{\mathbf{p}}_{1+}^i\hat{\mathbf{p}}_{1+}^i)e^{iw_1^id^+}\cdot\int e^{-iw_1^iz'}\mathcal{P}(z')\mathrm{d}z'.$$

$$\bar{\mathbf{E}}^-(d^+)=\mathcal{F}'_{h-}(\kappa^i)e^{-iw_1^id^+}.$$

while

$$\bar{\mathbf{E}}^+(0^l)=\mathcal{F}'_{h+}(\kappa^i)e^{iw_1^i0^l}.$$

$$\bar{\mathbf{E}}^-(0^l)=\mathcal{F}'_{h-}(\kappa^i)e^{-iw_1^i0^l} +\frac{i\tilde{\omega}^2}{2\epsilon_0w_1^i}(\hat{\mathbf{s}}^i\hat{\mathbf{s}}^i+\hat{\mathbf{p}}_{1-}^i\hat{\mathbf{p}}_{1-}^i)e^{-iw_1^i0^l}\cdot\int e^{iw_1^iz'}\mathcal{P}(z')\mathrm{d}z'.$$

where

$$\mathcal{F}'_{h+}(\kappa^i)=\mathcal{F}_{h+}+\frac{i\tilde{\omega}^2}{2\epsilon_0w_1^i}(\hat{\mathbf{s}}^iR_{1N}^s(\kappa^i)\hat{\mathbf{s}}^i +\hat{\mathbf{p}}_{1+}^iR_{1N}^p(\kappa^i)\hat{\mathbf{p}}_{1-}^i)\cdot\int e^{iw_1^iz'}\mathcal{P}(z')\mathrm{d}z'$$
$$\mathcal{F}'_{h-}(\kappa^i)=\mathcal{F}_{h-}.$$

Finally, we simplify these expressions by noting that $w_1^id\ll 1$ according to Eq. (11), and so recalling Eq. (18) we find Eq. (61), recalling that there we have put $\kappa^i\to\kappa$.

APPENDIX E: SURFACE EXCITATIONS AND FRESNEL COEFFICIENTS

In a multilayer structure, excitations of the electromagnetic field that propagate perpedicular to the growth direction are signaled by poles in the Fresnel coefficients of the structure. In this appendix we tabulate a few of the expressions that are relevant for surface plasmon and WG mode excitations.

We begin with a simple interface between a medium of relative permittivity $\varepsilon_1=n_1^2$ for $z>0$ and a metal with relative permittivity ε_m for $z<0$; we assume that $\mathrm{Re}\,\varepsilon_m$ is large and negative, and n_1 is real. The Fresnel coefficients for p-polarized light are given by Eq. (B4),

$$r^p_{1m} = \frac{w_1\varepsilon_m - w_m\varepsilon_1}{w_1\varepsilon_m + w_m\varepsilon_1},$$
$$t^p_{1m} = \frac{2n_1n_m w_1}{w_1\varepsilon_m + w_m\varepsilon_1}, \tag{E1}$$

where $n_m = \sqrt{\varepsilon_m}$, and throughout we use the square root convention introduced after Eq. (37). These coefficients have a pole at $\kappa = \kappa_{\rm SP}$, where

$$\kappa_{\rm SP} = \tilde{\omega}\sqrt{\frac{\varepsilon_m\varepsilon_1}{\varepsilon_m + \varepsilon_1}}, \tag{E2}$$

with $\tilde{\omega} = \omega/c$, identifies the surface plasmon excitation. The inverse of the Fresnel coefficients [Eq. (E1)] vanish at $\kappa = \kappa_{\rm SP}$ and thus are proportional to $\kappa - \kappa_{\rm SP}$ for κ close to $\kappa_{\rm SP}$. Performing the expansions, we find that for κ close to $\kappa_{\rm SP}$ we have

$$r_{1m} \approx \frac{\rho_{1m}}{\kappa - \kappa_{\rm SP}},$$
$$t_{1m} \approx \frac{\tau_{1m}}{\kappa - \kappa_{\rm SP}},$$

where the constants

$$\rho_{1m} = \frac{2w_1^{\rm SP}(w_m^{\rm SP})^2\varepsilon_1}{\kappa_{\rm SP}(w_m^{\rm SP}\varepsilon_m + w_1^{\rm SP}\varepsilon_1)},$$
$$\tau_{1m} = -\frac{2n_1n_m(w_1^{\rm SP})^2 w_m^{\rm SP}}{\kappa_{\rm SP}(w_m^{\rm SP}\varepsilon_m + w_1^{\rm SP}\varepsilon_1)}, \tag{E3}$$

and $w_1^{\rm SP}$ and $w_m^{\rm SP}$ are the values of w_1 and w_m, respectively, at $\kappa = \kappa_{\rm SP}$,

$$w_1^{\rm SP} \equiv \sqrt{\tilde{\omega}^2\varepsilon_1 - \kappa_{\rm SP}^2} = \tilde{\omega}\sqrt{\frac{\varepsilon_1^2}{\varepsilon_m + \varepsilon_1}},$$
$$w_m^{\rm SP} \equiv \sqrt{\tilde{\omega}^2\varepsilon_m - \kappa_{\rm SP}^2} = \tilde{\omega}\sqrt{\frac{\varepsilon_m^2}{\varepsilon_m + \varepsilon_1}}.$$

The expressions for a planar WG are slightly more complicated. We take a cladding with index n_1 for $z > 0$, a guide material with index n_2 for $0 > z > -D$, and a substrate with index n_3 for $z < -D$; we assume the three indices are real, with $n_2 > n_3 \geq n_1$. The Fresnel reflection (transmission) coefficient R_{13} (T_{13}) for a field incident from the cladding is given by the Airy formula,

$$T_{13} = \frac{t_{12}t_{23}e^{iw_2D}}{1 - r_{21}r_{23}e^{2iw_2D}},$$
$$R_{13} = \frac{r_{12} + r_{23}e^{2iw_2D}}{1 - r_{21}r_{23}e^{2iw_2D}}, \tag{E4}$$

where the fundamental reflection (transmission) coefficients r_{ij} (t_{ij}) are given by Eqs. (B3) and (B4) for s- and p-polarized light. In either case, WG modes are signaled by the poles of T_{13} and R_{13}:

$$1 - r_{21}r_{23}e^{2iw_2D} = 0.$$

After a little algebra, with the assumption that the n_i are real, this condition can be written as

$$\cot(hD) = \frac{h - \frac{PQ}{h}}{Q + P}, \tag{E5}$$

where

$$h = \sqrt{\tilde{\omega}^2n_2^2 - \kappa^2},$$
$$Q = a_Q\sqrt{\kappa^2 - \tilde{\omega}^2n_1^2},$$
$$P = a_P\sqrt{\kappa^2 - \tilde{\omega}^2n_3^2},$$

with

$$a_Q = a_P = 1 \quad (s - \text{polarized}),$$
$$a_Q = \frac{n_2^2}{n_1^2}, \quad a_P = \frac{n_2^2}{n_3^3} \quad (p - \text{polarized}). \tag{E6}$$

Equation (E5) implicitly determines the values κ_o of κ at which R_{13} and T_{13} diverge. It is the standard dispersion equation for WG modes, usually derived by writing down fields in the different regions and explicitly demanding that the Maxwell *saltus* conditions are satisfied across each interface [37]; of course, those conditions are implicitly guaranteed when the expressions for the Fresnel coefficients are constructed. Writing Q and P in terms of the refractive indices and h, the numerical solution of Eq. (E5) is facilitated by the fact that the left-hand side of the equation is a decreasing function of h, while the right-hand side is an increasing function of h. Near one of the κ_o the inverse of each of R_{13} and T_{13} is proportional to $\kappa - \kappa_o$, and working out the terms we find

$$R_{13} \approx \frac{\rho_{13}}{\kappa - \kappa_o},$$
$$T_{13} \approx \frac{\tau_{13}}{\kappa - \kappa_o},$$

where

$$\rho_{13} = \frac{2h_o^2Q_o}{\kappa_o D_{\rm eff}(h_o^2 + Q_o^2)},$$
$$\tau_{13} = \frac{2h_o^2Q_o a_{13}}{\kappa_o D_{\rm eff}\sqrt{(h_o^2 + Q_o^2)(h_o^2 + P_o^2)}}, \tag{E7}$$

with h_o, Q_o, and P_o indicating the values of those variables at $\kappa = \kappa_o$,

$$a_{13} = 1 \quad (s - \text{polarized}),$$
$$a_{13} = \frac{n_1}{n_3} \quad (p - \text{polarized}),$$

$$D_{\rm eff} = D + Q_o^{-1}\left(\frac{a_Q^2h_o^2 + Q_o^2}{h_o^2 + Q_o^2}\right) + P_o^{-1}\left(\frac{a_P^2h_o^2 + P_o^2}{h_o^2 + P_o^2}\right).$$

ACKNOWLEDGMENTS

We acknowledge the support from the Natural Sciences and Engineering Research Council of Canada (NSERC), through

both its Discovery Grants program and the NSERC Strategic Network for Bioplasmonic Systems. Computations were performed on the Compute Canada (SharcNet) supercomputing network.

REFERENCES

1. W. Lukosz and K. Tiefenthaler, "Directional switching in planar waveguides effected by absorbtion-desorbtion processes," in *Proceedings of the Second European Conference of Integrated Optics*, IEE Conference Publication No. 227 (IEE, 1983), pp. 152–155.
2. H. Mukundan, A. S. Anderson, W. K. Grace, K. M. Grace, N. Hartman, J. S. Martinez, and B. I. Swanson, "Review: waveguide-based biosensors for pathogen detection," Sensors **9**, 5783–5809 (2009).
3. C. Yu and J. Irudayaraj, "A multiplex biosensor using gold nanorods," Anal. Chem. **79**, 572–579 (2007).
4. A. Ulman, *An Introduction to Ultrathin Films* (Academic, 1991).
5. U. Kreibig and M. Vollmer, *Optical Properties of Metal Clusters* (Springer, 1995).
6. C. J. Kiely, J. Fink, M. Burst, D. Bethell, and D. J. Schiffrin, "Spontaneous ordering of bimodal ensembles of nanoscopic gold clusters," Nature **396**, 444–446 (1998).
7. A. J. Haes, D. A. Stuart, S. Nie, and R. P. Van Duyne, "Using solution phase nanoparticles, surface-confined nanoparticle arrays, and single nanoparticles as biological sensing platforms," J. Flouresc. **14**, 355–367 (2004).
8. S. Busse, J. Käshammer, S. Krämer, and S. Mittler, "Gold and thiol surface functionalized integrated optical Mach–Zehnder interferometer for sensing purposes," Sens. Actuators B **60**, 148–154 (1999).
9. K. A. Willets and R. P. van Duyne, "Localized surface plasmon resonance spectroscopy and sensing," Ann. Rev. Phys. Chem. **58**, 267–297 (2007).
10. Z. M. Qi, N. Matsuda, J. Santos, T. Yoshida, A. Takatsu, and K. Kato, "In situ monitoring of metal nanoparticle self-assembly on protein-functionalized glass by broadband optical waveguide spectroscopy," J. Colloid. Interface Sci. **271**, 249–253 (2004).
11. A. K. A. Aliganga, I. Lieberwirth, G. Glasser, A.-S. Duwez, Y. Sun, and S. Mittler, "Fabrication of equally oriented pancake shaped gold nanoparticles by SAM templated OMCVD and their optical response," Org. Electron. **8**, 161–174 (2007).
12. P. Rooney, A. Rezaee, S. Xu, T. Manifar, A. Hassanzadeh, G. Podoprygorina, V. Böhmer, C. Rangan, and S. Mittler, "Control of surface plasmon resonances in dielectrically-coated proximate gold nanoparticles immobilized on a substrate," Phys. Rev. B **77**, 235446 (2008).
13. S. M. Hashemi Rafsanjani, T. Cheng, C. Rangan, and S. Mittler, "A novel biosensing approach based on linear arrays of immobilized gold nanoparticles," J. Appl. Phys. **107**, 094303 (2010).
14. H. Jiang, T. Manifar, J. Sabarinathan, and S. Mittler, "3-D FDTD analysis of gold nanoparticle based photonic crystal on slab waveguide," J. Lightwave Technol. **27**, 2264–2270 (2009).
15. S. Mittler, "Gold nanoparticles on waveguides for and toward sensing application," in *Optical Guided-wave Chemical and Biosensors I*, M. Zourob and A. Lakhtakia, eds., Springer Series on Chemical Sensors and Biosensors (Springer, 2010), Vol. **7**, Part 2, pp. 209–229.
16. J. E. Sipe and J. Becher, "Surface energy transfer enhanced by optical cavity excitation: a pole analysis," J. Opt. Soc. Am. **72**, 288–295 (1982).
17. J. E. Sipe, "Bulk-selvedge coupling theory for the optical properties of surfaces," Phys. Rev. B **22**, 1589–1599 (1980).
18. G. A. Wurtz, J. S. Im, S. K. Gray, and G. P. Wiederrecht, "Optical scattering from isolated metal nanoparticles and arrays," J. Phys. Chem. B **107**, 14191–14198 (2003).
19. L. Zhao, K. L. Kelly, and G. C. Schatz, "The extinction spectra of silver nanoparticle arrays: influence of array structure on plasmon resonance wavelength and widths," J. Phys. Chem. B **107**, 7343–7350 (2003).
20. V. A. Markel, "Coupled-dipole approach to scattering of light from a one-dimensional periodic dipole structure," J. Mod. Opt. **40**, 2281–2291 (1993).
21. T. D. Backes and D. S. Citrin, "Plasmon polaritons in 2-D nanoparticle arrays," IEEE J. Sel. Top. Quantum Electron. **14**, 1530–1535 (2008).
22. Y.-R. Zhen, K. H. Fung, and C. T. Chan, "Collective plasmonic modes in two-dimensional periodic arrays of metal nanoparticles," Phys. Rev. B **78**, 035419 (2008).
23. S. M. R. Z. Bajestani, M. Shahabadi, and N. Talebi, "Analysis of plasmon propagation along a chain of metal nanospheres using the generalized multipole technique," J. Opt. Soc. Am. B **28**, 937–943 (2011).
24. E. Simsek, "On the surface plasmon resonance modes of metal nanoparticle chains and arrays," Plasmonics **4**, 223–230 (2009).
25. A. Semichaevsky and A. Akyurtlu, "Homogenization of metamaterial-loaded substrates and superstrates for antennas," Prog. Electromagn. Res. PIER **71**, 129–147 (2007).
26. A. A. Krokhin, P. Halevi, and J. Arriaga, "Long-wavelength limit homogenization for two-dimensional photonic crystals," Phys. Rev. B **65**, 115208 (2002).
27. Y. Wu and Z.-Q. Zhang, "Dispersion relations and their symmetry properties of electromagnetic and elastic metamaterials in two dimensions," Phys. Rev. B **79**, 195111 (2009).
28. P. A. Belov and C. R. Simovski, "Homogenization of electromagnetic crystals formed by uniaxial resonant scatterers," Phys. Rev. E **72**, 026615 (2005).
29. J. V. Kranendonk and J. E. Sipe, "Foundations of the macroscopic electromagnetic theory of dielectric solids," in *Progress in Optics XV*, E. Wolf, ed. (North-Holland, 1977), pp. 247–350.
30. J. D. Jackson, *Classical Electrodynamics*, 3rd ed. (Wiley, 1999).
31. J. E. Sipe, "New Green function formalism for surface optics," J. Opt. Soc. Am. B **4**, 481–489 (1987).
32. A. Bagchi, R. G. Barrera, and R. Fuchs, "Local-field effect in optical reflectance from adsorbed overlayers," Phys. Rev. B **25**, 7086–7096 (1982).
33. P. B. Johnson and R. W. Christy, "Optical constants of the noble metals," Phys. Rev. B **6**, 4370–4379 (1972).
34. H. C. van de Hulst, *Light Scattering by Small Particles* (Dover, 1981).
35. P. Berini, "Bulk and surface sensitivities of surface plasmon waveguides," New J. Phys. **10**, 105010 (2008).
36. J. E. Sipe, "The dipole antenna problem in surface physics: a new approach," Surf. Sci. **105**, 489–504 (1981).
37. A. Yariv, *Quantum Electronics*, 3rd ed. (Wiley, 1989).